Embryonic Protein NODAL Regulates the Breast Tumour Microenvironment by Reprogramming Cancer-Derived Secretomes

Dylan Dieters-Castator[1], Paola Marino Dantonio[2], Matt Piaseczny[1], Guihua Zhang[3], Jiahui Liu[3], Miljan Kuljanin[4,5], Stephen Sherman[4,6], Michael Jewer[1,3], Katherine Quesnel[6], Eun Young Kang[7], Martin Köbel[7], Gabrielle M. Siegers[3], Andrew Leask[6], David Hess[4,6], Gilles Lajoie[5], Lynne-Marie Postovit[2,3*]

[1]Department of Anatomy and Cell Biology, University of Western Ontario, London ON, Canada; [2]Department of Biomedical and Molecular Sciences, Queen's University, Kingston ON, Canada; [3]Department of Oncology, University of Alberta, Edmonton AB, Canada; [4]Robarts Research Institute, London ON, Canada; [5]Department of Biochemistry, University of Western Ontario, London ON, Canada; [6]Department of Physiology and Pharmacology, University of Western Ontario, London ON, Canada; and [7]Department of Pathology and Laboratory Medicine, University of Calgary, Foothills Medical Centre, Calgary, AB, Canada;

*To whom correspondence should be addressed: Lynne-Marie Postovit, 563 Botterell Hall, Queen's University, Kingston ON, Canada, K7L 2V7; l.postovit@queensu.ca

Abstract

The tumour microenvironment (TME) is an important mediator of breast cancer progression. Cancer-associated fibroblasts (CAFs) constitute a major component of the TME and may originate from tissue-associated fibroblasts or infiltrating mesenchymal stromal cells (MSCs). The mechanisms by which cancer cells activate fibroblasts and recruit MSCs to the TME are largely unknown, but likely include deposition of a pro-tumourigenic secretome. The secreted embryonic protein NODAL is clinically associated with breast cancer stage and promotes tumour growth, metastasis, and vascularization. Herein, we show that NODAL expression correlates with the presence of activated fibroblasts in human triple negative breast cancers and that it directly induces CAF phenotypes. We further show that NODAL reprograms cancer cell secretomes by simultaneously altering levels of chemokines (e.g. CXCL1), cytokines (e.g. IL-6) and growth factors (e.g. PDGFRA), leading to alterations in MSC chemotaxis. We therefore demonstrate a hitherto unappreciated mechanism underlying the dynamic regulation of the TME.

Introduction

Solid malignancies contain many non-transformed stromal cell types within the tumour microenvironment (TME). In breast cancer, a significant proportion of auxiliary cells, including cancer-associated fibroblasts (CAFs), pericytes, myoepithelial and endothelial cells, tumour-associated macrophages (TAMs) and other immune cell types, cooperate to promote pro-tumorigenic processes such as metastasis and drug resistance[1-3]. Dramatic gene expression changes in stromal cells are associated with the transformation of normal breast tissue to ductal carcinoma *in situ* (DCIS)[4,5], and progression from DCIS to invasive ductal carcinoma (IDC) is marked by upregulated expression of extracellular matrix (ECM)-degrading proteases[5], revealing an important role of TME components in breast cancer initiation and progression.

Among TME cell types, CAFs constitute the major stromal component of many breast cancers and have recently emerged as potential therapeutic targets[6-8]. Fibroblasts are the main producers of ECM and play fundamental roles in tissue repair, during which they acquire an activated myofibroblast phenotype characterized by α-smooth muscle actin (α-SMA) expression[9,10]. Fibroblasts are highly responsive to their microenvironment, interacting with and influencing a wide range of cells. For example, fibroblasts promote angiogenesis through the secretion of vascular endothelial growth factor A (VEGFA)[11], coordinate immune response through cytokine and chemokine release[12,13], and influence epithelial stem cells[14,15]. Ligands from the transforming growth factor beta (TGF-β) family are well-known fibroblast activators[16,17], as are cytokines[18] and ECM remodelling[19,20]. Extracellular factors, such as cytokines and ECM proteins, mediate the pro-tumorigenic behaviours of CAFs. For instance, CAF-derived CXCL12/stromal derived factor (SDF-1) can mobilize endothelial progenitor cells (EPCs) to increase vascularization of MCF-7 xenografts[21]. Moreover, subsets of CAFs can increase tumorigenesis and breast cancer stem cell (BCSC) enrichment by secreting interleukins (IL) IL-6, IL-8 and IL-1β[6,7,22]. Several recent studies have demonstrated that CAFs are heterogeneous and can be derived through activation of tissue-

associated fibroblasts[23], as well as the recruitment of mesenchymal stromal cells (MSCs)[24,25]. In fact, up to 20% of CAFs were derived from MSCs in a CXCL6/CXCR6-dependent manner in a mouse model of gastric cancer[26]. An orthotopic breast cancer model revealed that MSCs can be recruited to primary tumour sites and that TGF-β1 is involved in this process[27]. MSCs also acquire CAF-like phenotypes when cultured in tumour conditioned media or mixed with cancer cells in mouse xenografts[28-30]. The mechanisms underlying MSC recruitment are not fully understood, but it is becoming increasingly clear that this population may contribute to the CAF compartment in the TME.

Limited genetic alterations have been described in breast cancer-associated stromal cells[31-34], suggesting that changes in gene expression observed in these cells are mainly due to epigenetic reprogramming[35,36]. For instance, breast cancer cells induce fibroblasts to secrete the ECM protein degrader ADAMTS1 through epigenetic changes[37], demonstrating that the epigenetic reprogramming in stromal cells can be induced by cancer cells. The cancer secretome plays a vital role in the pro-tumorigenic effects of the TME, recruiting stromal cells and reprogramming them to support tumour progression[38-40].

Several studies have uncovered tumour promoting roles for the secreted TGF-β superfamily member and embryonic morphogen NODAL[41,42]. NODAL expression, while primarily restricted to embryonic development and human embryonic stem cells (hESCs), has been observed in melanoma, glioblastoma, breast, pancreatic and hepatocellular cancers, amongst others[42,43]. In breast cancer, NODAL clinically correlates with stage and vascularization[44,45]. Moreover, NODAL expression emerges in breast cancers as they transition from DCIS into IDC[46], wherein interactions between cancer and stromal cells are critical. NODAL inhibition reduces breast cancer-induced neovascularization and mitigates BCSC frequencies, tumour growth, and invasion[47-49]. NODAL may also play an essential role in remodeling the TME. For example, NODAL seems to induce a breast cancer secretome that promotes angiogenesis through

regulation of the angiogenic factors platelet-derived growth factor (PDGF) and vascular endothelial growth factor (VEGF)[45]. Furthermore, NODAL expression is inversely correlated with susceptibility to gamma delta (γδ) T cell cytotoxicity, at least in part through decreased surface expression of the immune activating danger signal MHC class I polypeptide-related sequence A/B (MICA/B)[50]. CAFs from a gastric cancer mouse model have recently been shown to promote cancer cell proliferation and resistance to doxorubicin via NODAL secretion[51] and NODAL appears to induce CAF-like phenotypes in mouse and human fibroblast cell lines[52]. The extent to which NODAL may affect CAF phenotypes in the breast TME has not, however, been explored.

In this study, we investigated the impact of NODAL on CAFs and MSCs within the triple negative breast cancer (TNBC) TME. We demonstrate that NODAL strongly correlates with CAFs in breast cancer patients and that this morphogen can directly signal to fibroblasts (but not to MSCs) to induce a CAF-associated phenotype. In addition, mass spectrometry-based proteomics of conditioned media derived from triple negative MDA-MB-231 and triple negative inflammatory SUM149 breast cancer cells demonstrated that NODAL is a potent regulator of the breast cancer secretome. Our analyses revealed cancer cell-type-specific alterations in several novel NODAL-regulated factors, including CXCL1, CXCL8, IL-6 and colony-stimulating factor 1 (CSF1), suggesting that NODAL may impact the ability of breast cancer cells to recruit a variety of stromal cell types. Accordingly, we found that MSC chemotaxis towards breast cancer cells is affected by NODAL-regulated factors such as IL-6. Collectively, these data reveal a previously unknown role for NODAL in the regulation of breast cancer TME.

Results

Cancer cells expressing NODAL associate with α-SMA-positive stromal cells in triple negative breast tumors

Because fibroblast activation (demarcated by α-SMA expression) and NODAL expression occur early during breast cancer progression[46], we investigated whether these events could be correlated. We evaluated the expression and localization of NODAL and α-SMA in 41 primary tumour tissue samples from a cohort of 20 TNBC cases (**Table I**). Representative images are shown in **Fig. 1**. NODAL expression was observed in 92.7% of samples (38/41) (**Table I**), while α-SMA was detected in all slides. Stromal-associated α-SMA (**Fig. 1b, d**) was observed in all 38 NODAL-positive samples and the intensity of α-SMA staining was found to be increased in 94.7% (36/38) of regions with NODAL-positive cells as compared to NODAL-negative regions (**Table I**). Notably, α-SMA was also detected in areas that were negative for NODAL; however, in these instances, α-SMA delineated myoepithelial cells (**Fig. 1e, f**). Overall, these results reveal a strong association between NODAL and α-SMA expression in the stroma of TNBC patients, suggesting NODAL could have an impact on CAF phenotypes in breast cancer.

143 **Table I.** NODAL and α-SMA evaluation by immunohistochemistry.

	n (%)
NODAL score – Median (range)	2 (0-3)
0	3 (7.3)
1	10 (24.4)
2	19 (46.3)
3	9 (22.0)
NODAL percentage (%) – Median (range)	50 (5-100)
NA	3 (7.3)
5-20	12 (29.3)
30-40	7 (17.1)
60-80	14 (34.1)
90-100	5 (12.2)
NODAL distribution	
NA	3 (7.3)
Diffuse	17 (41.5)
Scattered	20 (48.8)
Focal	1 (2.4)
α-SMA score – Median (range)	2 (1-3)
1	3 (7.3)
2	29 (70.7)
3	9 (22.0)
Intensity Association	
NA	3 (NA)
Yes	36 (94.7)
No	2 (5.3)

144

145

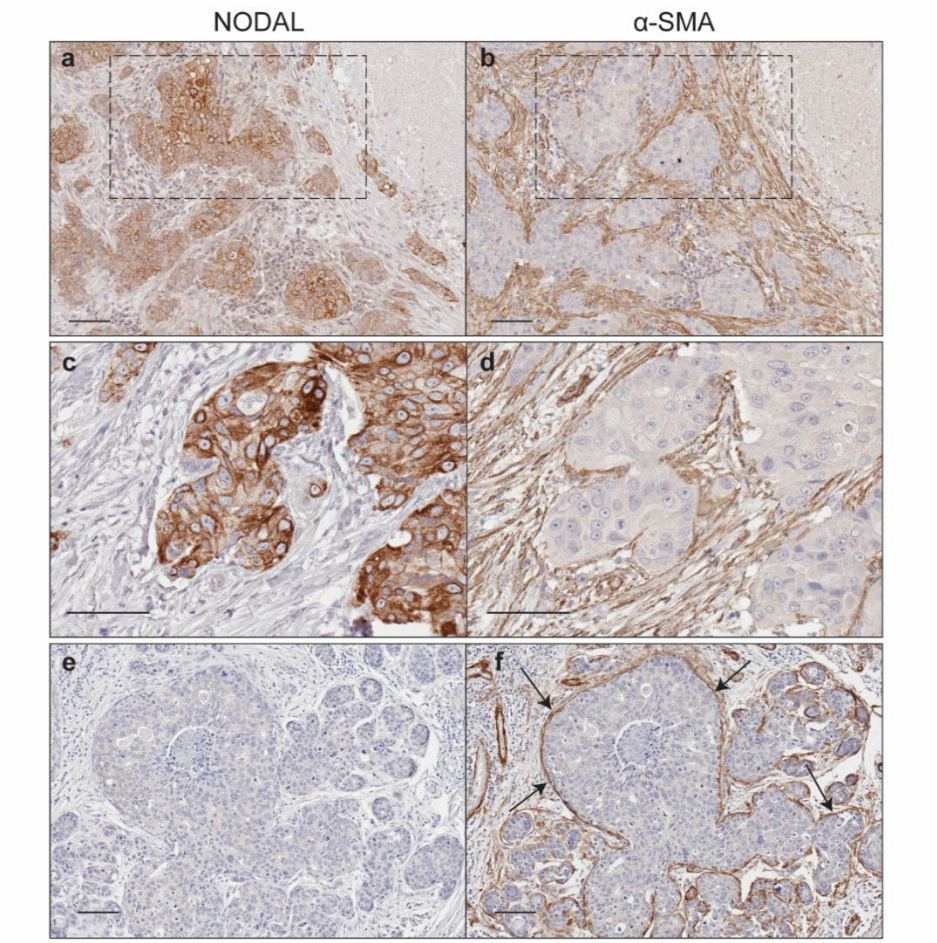

Figure 1. Breast cancer cells expressing NODAL reside adjacent to α-SMA-positive stromal cells. Representative images are shown wherein NODAL (a, c, e) and α-SMA (b, d, f) are stained in serial sections of tissue from triple negative breast cancer patients. **(a-d)** NODAL-positive breast cancer cells are surrounded by diffuse α-SMA+ stromal cells (for example in square). **(e, f)** In NODAL-negative sections, α-SMA is localized only to basement membranes (arrows). Bar equals 100 μm.

NODAL induces fibroblast activation and chemotaxis

Since we found a consistent spatial association between NODAL and stromal α-SMA in human TNBC tissues, we decided to examine whether NODAL affects, directly or indirectly, breast cancer-induced fibroblast phenotypes (**Fig. 2**). MDA-MB-231 TNBC cells express high basal levels of NODAL, therefore we investigated if serum-free conditioned media (CM) of MDA-MB-231 cells stably expressing scrambled control (shControl) or NODAL knockdown (shNODAL)

shRNA (**Fig. 2a**) can differentially impact primary fibroblasts. We also explored the effects of recombinant human NODAL (rhNODAL) on these cells. We detected a small, but statistically insignificant reduction in primary human foreskin fibroblast (HFF) chemotaxis towards CM from shNODAL versus shControl MDA-MB-231 cells (**Fig. 2b**), while rhNODAL (10 and 100 ng/mL) increased HFF chemotaxis (**Fig. 2c**), proliferation (**Fig. 2d**) and invasion (**Fig. 2e**). Further addressing fibroblast activation by NODAL, real-time RT-PCR revealed that rhNODAL (10 and 100ng/mL) induced expression of α-SMA, desmin, and connective tissue growth factor (CTGF) (**Fig. 2f**), which are CAF markers. In addition, we performed gene expression profiling on human dermal fibroblasts (HDFs) treated with 10ng/mL rhNODAL for 6h. Transcripts upregulated by at least 1.7 fold were analyzed in DAVID; gene clusters associated with the GO terms “wound healing”, “cell motion”, “extracellular matrix” and “growth factor” were significantly enriched (**Fig. 2g; Sup. Table 1**)[53], suggesting that fibroblasts are indeed activated by NODAL.

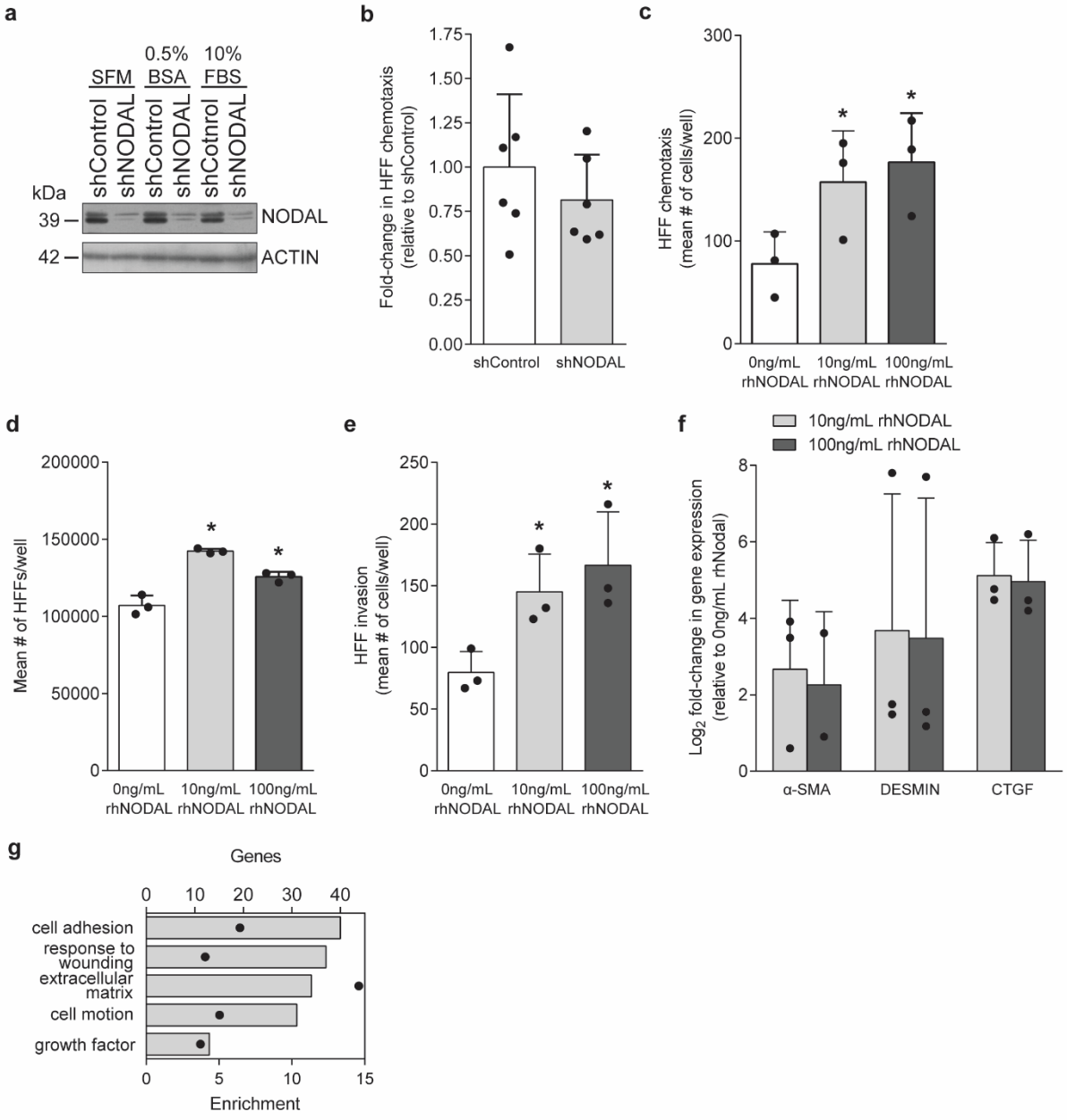

Figure 2. NODAL directly promotes phenotypes associated with activated fibroblasts in HFFs. (a) NODAL expression in MDA-MB-231 cells stably expressing scrambled (shControl) or NODAL knockdown (shNODAL) shRNA cultured in SFM, SFM+0.5%BSA (0.5%BSA), or complete media (10% FBS). **(b)** HFF chemotaxis towards CM from MDA-MB-231 cells (n=6). **(c-e)** Exposure to rhNODAL (10 and 100ng/mL) significantly increased HFF chemotaxis, proliferation, and invasion (n=3); Dunnett's multiple comparison test, *p<0.05. **(f)** HFFs upregulated transcripts (*a-SMA*, *DESMIN* and *CTGF*) associated with activated fibroblasts following treatment with rhNODAL (10 and 100ng/mL; n=3, n=2 for α-SMA from 100ng/mL treatment). **(g)** Total genes (bars) upregulated by NODAL (10ng/mL) more than 1.7-fold in human dermal fibroblasts (HDFs) and their corresponding enrichment (black dots) following GO analysis in DAVID.

The NODAL-regulated MDA-MB-231 secretome impacts MSC chemotaxis

The fibroblast population in breast cancer is highly heterogeneous and likely derived from different cell types[23,54]. Given the involvement of MSCs in tumour growth and neovascularization, and their probable contribution to the CAF population, we examined how NODAL affects the capacity of breast cancer cells to promote chemotaxis by comparing the ability of CM from shControl and shNODAL knockdown MDA-MB-231 cells to influence MSC chemotaxis (**Fig. 3**). Several primary human bone marrow-derived (BM-)MSC lines were utilized herein, some of which have been previously shown to form tubes *in vitro* and stimulate islet regeneration and revascularization *in vivo*[55,56]. In three out of four MSC lines, chemotaxis was significantly decreased (~1.8 to 3.5-fold) towards shNODAL CM as compared to shControl CM. We did not observe appreciable differences in proliferation or viability of MSCs cultured in CM for 24h, suggesting that the effects observed were not due to alterations in cell numbers, but rather a result of altered chemotaxis (**Sup. Fig. 1a**).

The reduction in MSC chemotaxis observed when NODAL was knocked down could not be rescued by the addition of 100ng/mL of rhNODAL (**Fig. 3a, b, d**) suggesting that MSCs are unable to sense this morphogen, perhaps due to an absence of receptor components. Hence, we performed real-time RT-PCR and western blotting for NODAL, its receptor (ALK4) and co-receptor (CRIPTO) on MSC lines (**Fig. 4a, b**). MSCs expressed moderate levels of NODAL and high levels of ALK4 at the transcript and protein level (**Fig. 4a, b**). *CRIPTO* mRNA expression approached the reliable limit of detection by quantitative real-time PCR (35 cycles) (**Fig. 4a**). Hence, while MSCs appear to make NODAL and to express NODAL receptors, they may not express enough CRIPTO to sense NODAL. Stimulation with 10 and 100 ng/mL rhNODAL did not affect canonical or non-canonical signalling through SMAD2 or ERK1/2 phosphorylation, respectively (**Fig. 4c**). In contrast to MSCs, which appeared unresponsive to NODAL, we found that rhNODAL (10 and

100ng/mL) caused an increase in both SMAD2 and ERK1/2 activation in fibroblasts (**Fig. 4d**), suggesting NODAL can directly promote fibroblast activation.

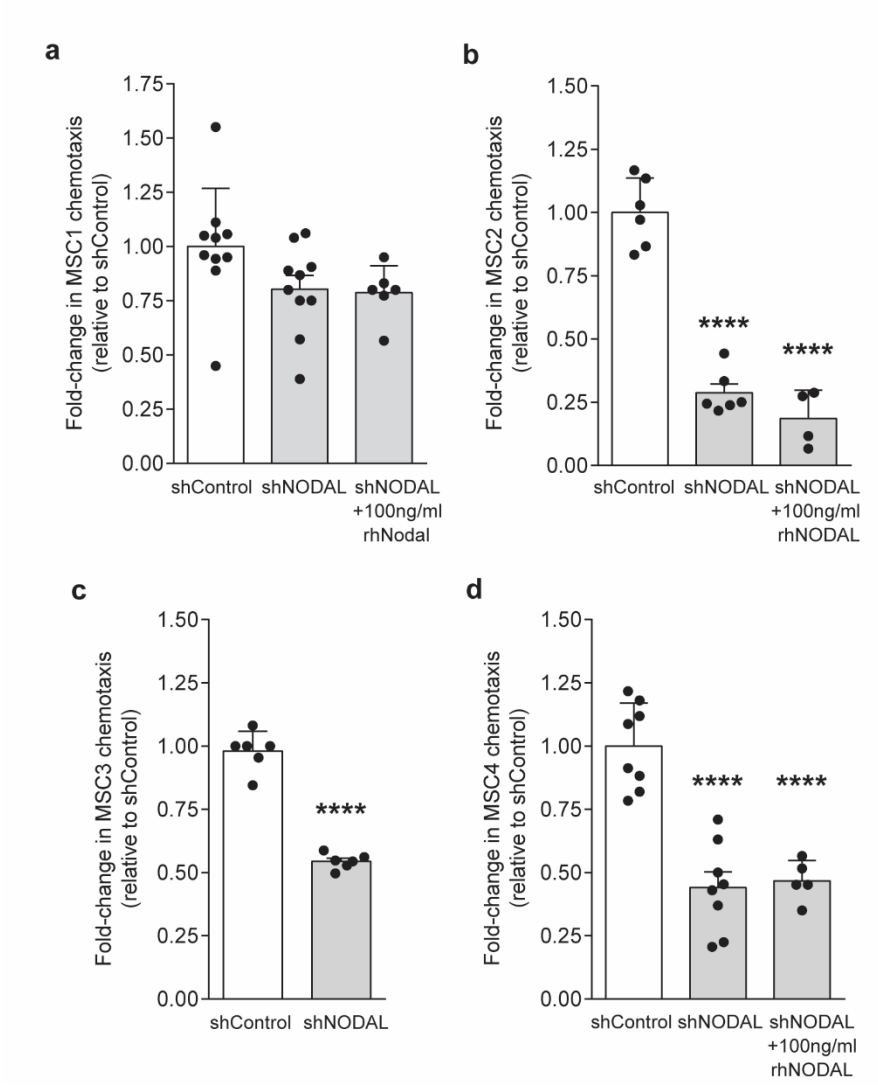

Figure 3. Conditioned media from NODAL-knockdown MDA-MB231 breast cancer cells indirectly modulates MSC chemotaxis. (a-d) Human bone-marrow derived MSC lines (MSC1-4) were plated onto fibronectin-coated transwells in the presence of CM (shControl or shNODAL +/-100ng/mL rhNODAL). MSC chemotaxis was significantly lower towards shNODAL CM compared to shControl CM after 24h and was not rescued by rhNODAL; ****p<0.0001, Dunnett's multiple comparison test.

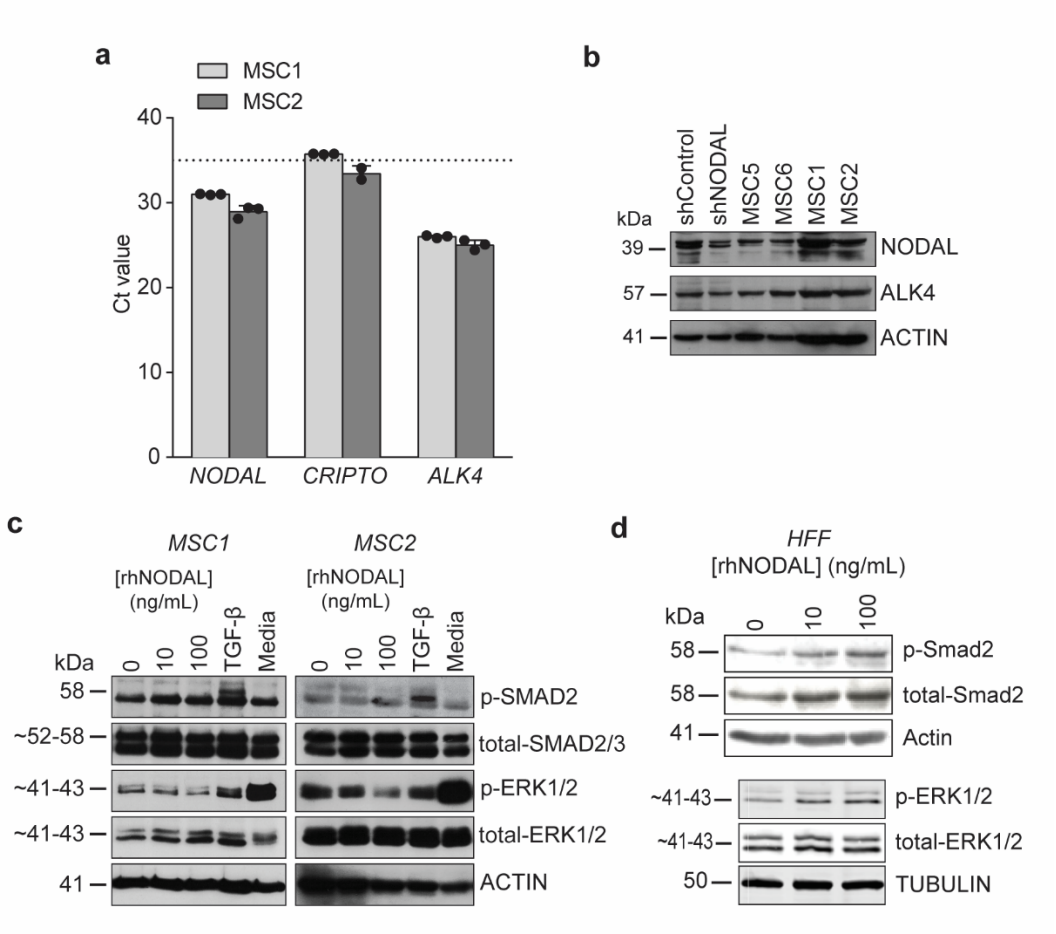

Figure 4. NODAL signalling in MSCs. (a) Real time PCR cycle threshold (Ct) values for *NODAL*, *ALK4* and *CRIPTO* in MSCs. Data are presented as mean Ct values ± SD from three biological replicates except for *CRIPTO* (n=2 for MSC2). High Ct values indicate low transcript expression with the horizontal dotted line corresponding to a Ct value of 35 or the reliable limit of detection. **(b)** Western blots showing expression of NODAL and ALK4 (receptor) in four MSC lines. shControl and shNODAL MDA-MB-231 cells were used as positive controls. **(c)** Serum-starved MSCs treated with varying concentrations of rhNODAL had no effect on downstream SMAD2 (p-SMAD2) or ERK1/2 (p-ERK1/2) activation. TGF- β treatment and cell culture media were used as positive controls for SMAD2 and ERK1/2 activation, respectively. **(d)** Stimulation of HFFs with rhNODAL activates SMAD2 and ERK1/2 phosphorylation in a dose-dependent fashion. Western blots are representative images taken from three biological replicates.

Modulation of NODAL expression alters the breast cancer secretome

Mass spectrometry is a powerful tool for proteomic characterization of cancer cell lines and tissues[57,58]. To further elucidate the mechanisms through which NODAL may influence stromal

cells, we employed high-resolution mass spectrometry to identify NODAL-regulated factors in serum-free CM from breast cancer cells. Stable isotopic labelling of amino acids in culture (SILAC) was combined with SDS-PAGE fractionation to determine relative changes in secreted proteins from shControl and shNODAL MDA-MB-231 cells. In total, this approach identified over 3200 proteins, which were reduced to ~1300 entries after filtering for proteins annotated with Gene Ontology Cellular Component (GOCC) terms containing "extracellular" and quantified in at least two out of three biological replicates (**Fig. 5a, Sup. Table 2**). Of those, 122 proteins were significantly different ($p<0.05$) between shControl and shNODAL CM (**Fig. 5a, Sup. Table 2**). From this list, 1D annotation enrichment in Perseus revealed a significant decrease in proteins involved in GO Biological Processes (GOBPs) associated with cell migration, inflammation and cytokine signalling following NODAL knockdown (**Fig. 5b, Sup. Table 3**)[59]. Alternatively, proteins matching to GOBP terms mRNA processes, protein localization and macromolecular complex disassembly were significantly increased. This observation was attributed to higher levels of ribosomal proteins (RPS and RPL members) shed by shNODAL MDA-MB-231 cells. We plotted Heavy/Light ratios (shNODAL/shControl) and their corresponding $-\log_{10}$ p-values for the ~1300 filtered extracellular proteins found in MDA-MB-231 CM (**Fig. 5c**). All proteins annotated with the aforementioned GOBP terms were highlighted in blue (depleted) or red (enriched); there was a clear trend towards a reduction in the secretion of inflammatory and chemotactic proteins following NODAL knockdown and an opposing increase in transcriptional and translational proteins. CXCL chemokines (CXCL1/3/8), IL-6 and CSF1 were significantly lower in shNODAL CM ($p<0.05$). Interleukin 11 (IL-11), on the other hand, was significantly higher (~1.85 fold, $p<0.05$). These factors have been associated with malignant phenotypes and may contribute to MSC chemotaxis given that they can promote chemotaxis of various immune cells and, in some cases, MSCs[60-62]. Similar to previous findings, PDGFA was significantly lower in shNODAL CM (-2.31 fold)[45]. Proteomic findings were verified by ELISAs with CM from MDA-MB-231 cells for

CXCL1, CXCL8, IL-6 and CSF1 (**Sup. Fig. 2a**). These results suggest that NODAL expression is associated with the secretion of inflammatory and chemotactic proteins by breast cancer cells.

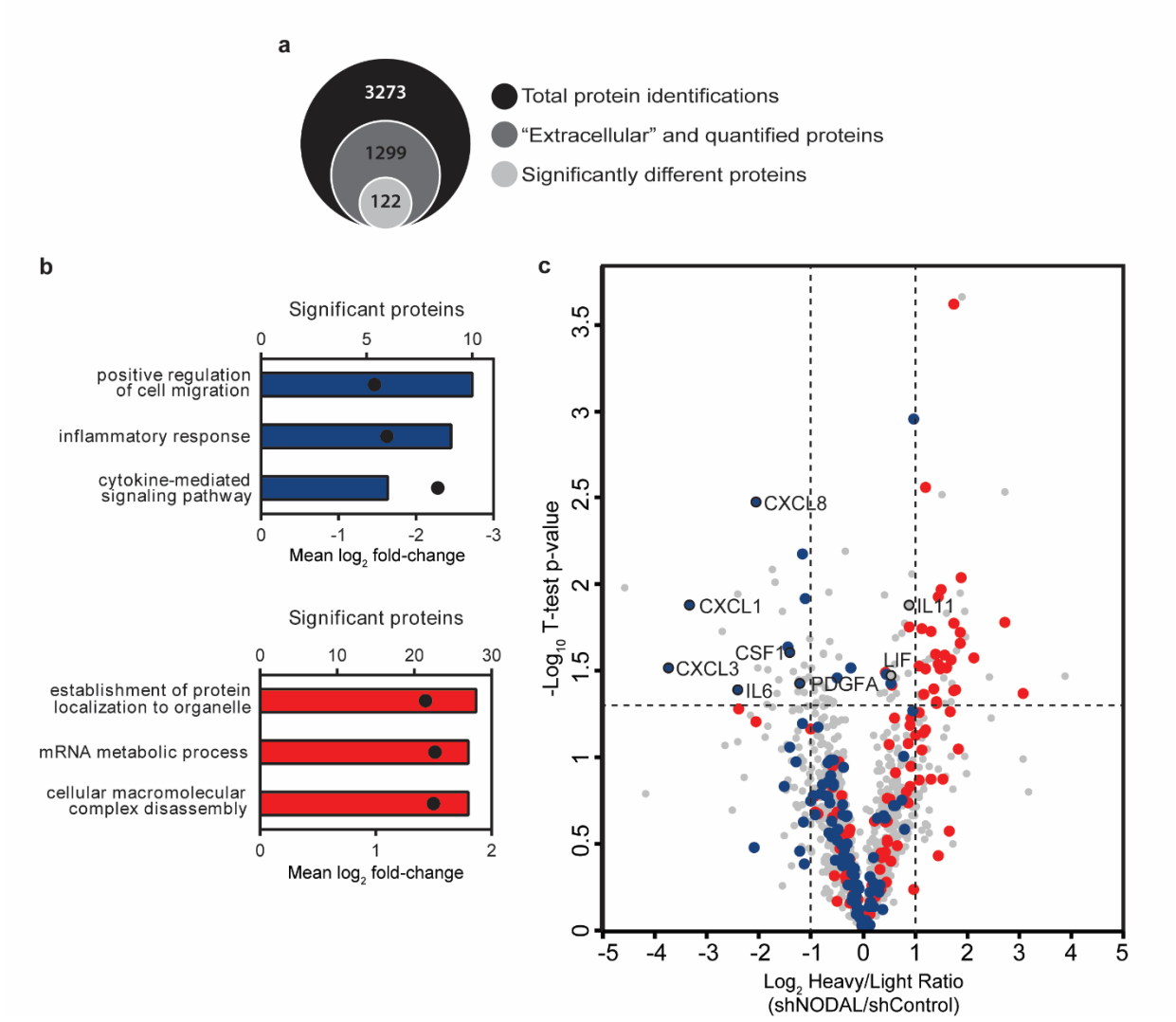

Figure 5. NODAL knockdown alters the MDA-MB-231 secretome. Extracellular proteins from serum-free shControl and shNODAL CM were analyzed by high-resolution mass spectrometry. **(a)** Venn diagram highlighting total protein identifications, number of "extracellular" and quantified proteins, and significantly different proteins between shControl and shNODAL CM (two-tailed, one sample t-test, $p<0.05$). **(b)** Number of significant proteins (bars) matching to a subset of significantly enriched (Benjamini Hochberg (BH) FDR threshold<0.02) GO biological processes (GOBPs). Mean log_2 fold-changes in GOBPs are indicated by black dots. Blue and red bars highlight GOBPs decreased and increased in MDA-MB-231 CM following NODAL knockdown, respectively. **(c)** Volcano plot of quantified "extracellular" proteins. Negative and positive Log_2 Heavy/Light ratios indicate proteins decreased and increased in MDA-MB-231 CM following NODAL knockdown, respectively (n=3). All proteins matching to corresponding GOBPs mentioned are

highlighted in blue and red. Several cytokines and chemokines altered by NODAL are labelled in black. Vertical and horizontal dotted lines indicate $\log_2$ fold-changes ≥2 and the $-\log_{10}$ p-value cut-off corresponding to $p<0.05$, respectively.

IL-6 promotes MSC chemotaxis

Given that NODAL consistently altered CXCL1 and IL-6 levels in MDA-MB-231 CM, which were associated with differential MSC chemotaxis, we sought to determine whether receptors for these ligands were expressed by MSCs. While three MSC lines were highly positive for IL-6R based on flow cytometry (**Fig. 6a; Sup. Fig. 3a, b**), surface CXCR1 and CXCR2 expression could not be detected in any of the MSC lines by real-time PCR or flow cytometry (**Sup. Fig. 3c**; data not shown). Accordingly, treatment with 10 and 25ng/mL recombinant human IL-6 (rhIL-6) induced STAT3 phosphorylation in MSC2 cells, which could be blocked by the addition of an IL-6 neutralizing monoclonal antibody (mAb, **Fig. 6b**). Moreover, low doses of rhIL-6 (1 and 10ng/mL) significantly increased MSC2 chemotaxis by ~1.6 fold ($p<0.05$) although higher concentrations had no effect (**Fig. 6c**). Neutralizing IL-6 in shControl CM resulted in a small, but significant, decrease in MSC2 chemotaxis (Fig. 6d), while supplementing shNODAL CM with rhIL-6 (1ng/mL) increased MSC2 chemotaxis (**Fig. 6e**). These findings suggest that IL-6 may be involved in promoting MSC recruitment to breast cancers.

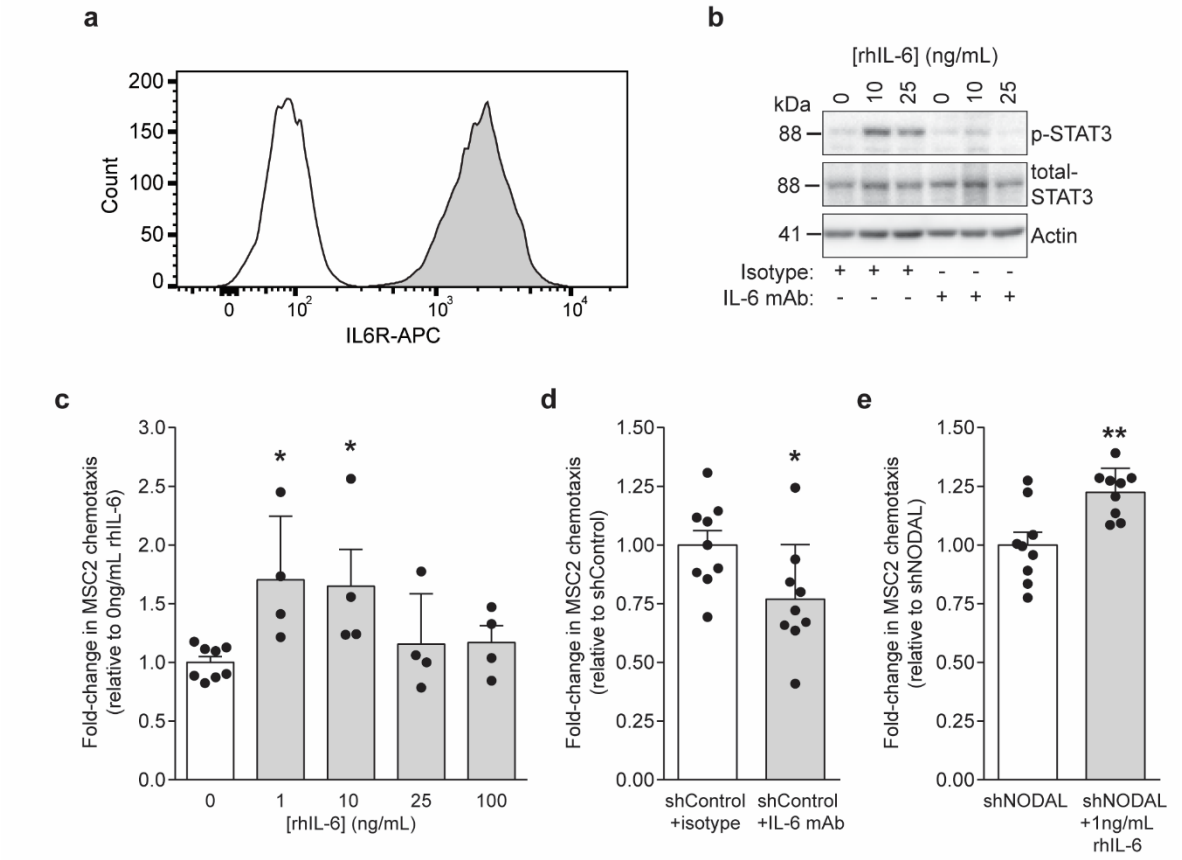

Figure 6. IL-6 contributes to MDA-MB-231 mediated MSC chemotaxis. (a) Flow cytometry showing nearly homogenous expression of the IL-6 receptor (IL-6R) by MSCs. **(b)** Stimulation with rhIL-6 induced phosphorylation of STAT3 in MSC2, which could be blocked by pre-incubation with an IL-6 neutralizing mAb. **(c)** MSC chemotaxis towards rhIL-6 after 24h (n=4-8). Low concentrations (1-10ng/mL) of rhIL-6 significantly induced MSC chemotaxis (Dunnett's multiple comparison test, *p<0.05). **(d)** IL-6 neutralizing mAb significantly attenuated MSC chemotaxis. **(e)** Exogenous rhIL-6 significantly increased MSC chemotaxis towards shNODAL CM. Flow histogram and western blots are representative images from three biological replicates. Data are presented as mean fold-changes relative to controls ± SD. Black dots indicate replicate values and asterisks indicate significance differences (one-way ANOVA, Dunnett's multiple comparison test for IL-6 dose response and two-tailed, two sample t-test for MDA-MB-231 treatments) in MSC chemotaxis compared to controls (* p<0.05, ** p<0.01).

NODAL-induced reprogramming of the breast cancer secretome is context-dependent

NODAL/ACTIVIN regulates cell fate specification and phenotype by activating signal transduction pathways that directly affect transcription and mediate epigenetic modifications[63]. The ability of

NODAL to broadly affect gene expression is context-dependent. Given that inflammatory breast cancer is marked by a discrete TME composition and function[64], tumour cells and TME components in this breast cancer subtype may well cooperate under distinct cellular and signalling contexts. Therefore, we investigated the impact of NODAL on the secretome of SUM149 triple negative inflammatory breast cancer cells, which express low levels of NODAL, to determine if it differs from that of MDA-MB-231 cells.

In contrast to the knockdown model previously employed in MDA-MB-231 cells, we generated NODAL-overexpressing and green fluorescent protein (GFP) control SUM149 cells from which Strong Cation Exchange (SCX)-fractionated CM digests were obtained for label-free quantitative proteomics (**Fig. 7a**). Approximately 1500 proteins were annotated as "extracellular" and quantified in at least two out of three biological replicates, and 344 proteins were significantly different between NODAL and GFP expressing SUM149 cells (**Fig. 7b, Sup. Table 4**). GOBPs that were significantly enriched or depleted included terms associated with inflammation, cell migration/locomotion, translation, and transcription (**Fig. 7c, Sup. Table 5**). Unexpectedly, GOBPs depleted in shNODAL MDA-MB-231 samples were also depleted in NODAL overexpressing SUM149 CM. For instance, proteins matching the cytokine-mediated signalling pathway had a mean $\log_2$ fold-change of -2.28 and -2.44 following NODAL knockdown and overexpression, respectively (**Fig. 5b and 7c**). Conversely, proteins matching "mRNA metabolic process" were increased significantly by NODAL knockdown in MDA-MB-231 and NODAL overexpression in SUM149 with mean $\log_2$ fold-changes of 1.51 and 1.88, respectively. We also plotted $\log_2$ protein fold-changes for SUM149 secretomes (NODAL-GFP) versus $-\log_{10}$ p-values and highlighted all proteins annotated with the aforementioned GOBPs (**Fig. 7d**). Several inflammatory and migratory factors decreased following NODAL overexpression while translational and transcriptional proteins were elevated. As in NODAL knockdown in MDA-MB-231 cells, CXCL1, CXCL3, IL-6 and CSF1 levels also decreased following NODAL

325 overexpression in SUM149 cells. Highly similar proteomic results were also observed when
326 comparing CM from NODAL overexpressing SUM149 cells to cells expressing an empty vector
327 (EV) (**Sup. Fig. 4 and Sup. Tables 6 and 7**). In total, 56 proteins were significantly altered by
328 NODAL in both MDA-MB-231 and SUM149 datasets; however, only a handful were associated
329 with NODAL expression in a positive (CLU and CLSTN3) and negative (leukemia inhibitory factor
330 [LIF] and neuropillin-2 [NRP2]) manner in both cell lines. Moreover, NODAL promoted a pro-
331 angiogenic phenotype in both MDA-MB-231 and SUM149 cells. For example, although PDGFA
332 was not detected in SUM149 CM, the angiogenic factors angiopoietin-1 (ANGPT1) and
333 angiogenin (ANG) were significantly elevated in CM from NODAL-overexpressing SUM149 cells
334 (Fig. 7d, Sup. Tables 4 and 6)[65,66].

335 In accordance with NODAL's ability to directly activate fibroblasts, CM from NODAL
336 overexpressing SUM149 cells significantly increased HFF chemotaxis compared to the GFP
337 expressing control (**Fig. 7e**). Furthermore, in line with results suggesting that NODAL affects MSC
338 chemotaxis indirectly by reprogramming the breast cancer secretome, CM derived from NODAL
339 overexpressing SUM149 cells induced less chemotaxis in MSC2 cells compared to CM from the
340 GFP expressing control cells (**Fig. 7f**). This reduced chemotaxis is likely attributable to lower
341 levels of cytokines such as IL-6. Again, we confirmed by flow cytometry that differences in
342 chemotaxis were not due to altered proliferation or viability (**Sup. Fig. 1b**; data not shown).

343 In a Venn diagram to assess relationships among differentially expressed proteins from MDA-
344 MB-231, HDF, and SUM149 proteomics and microarray datasets, we found several factors
345 consistently altered by NODAL, albeit some inversely correlated with NODAL levels (**Fig. 7g**). IL-
346 6, LIF, and NRP2 were shared amongst all three datasets; however, CXCL1/3 appeared to be
347 exclusively modulated in breast cancer cells. Hence, while NODAL indirectly affects MSC
348 chemotaxis by altering the breast cancer secretome, NODAL can directly induce fibroblast

activation. Moreover, certain key factors, such as IL-6 and LIF, are commonly affected by NODAL in all cell types investigated here.

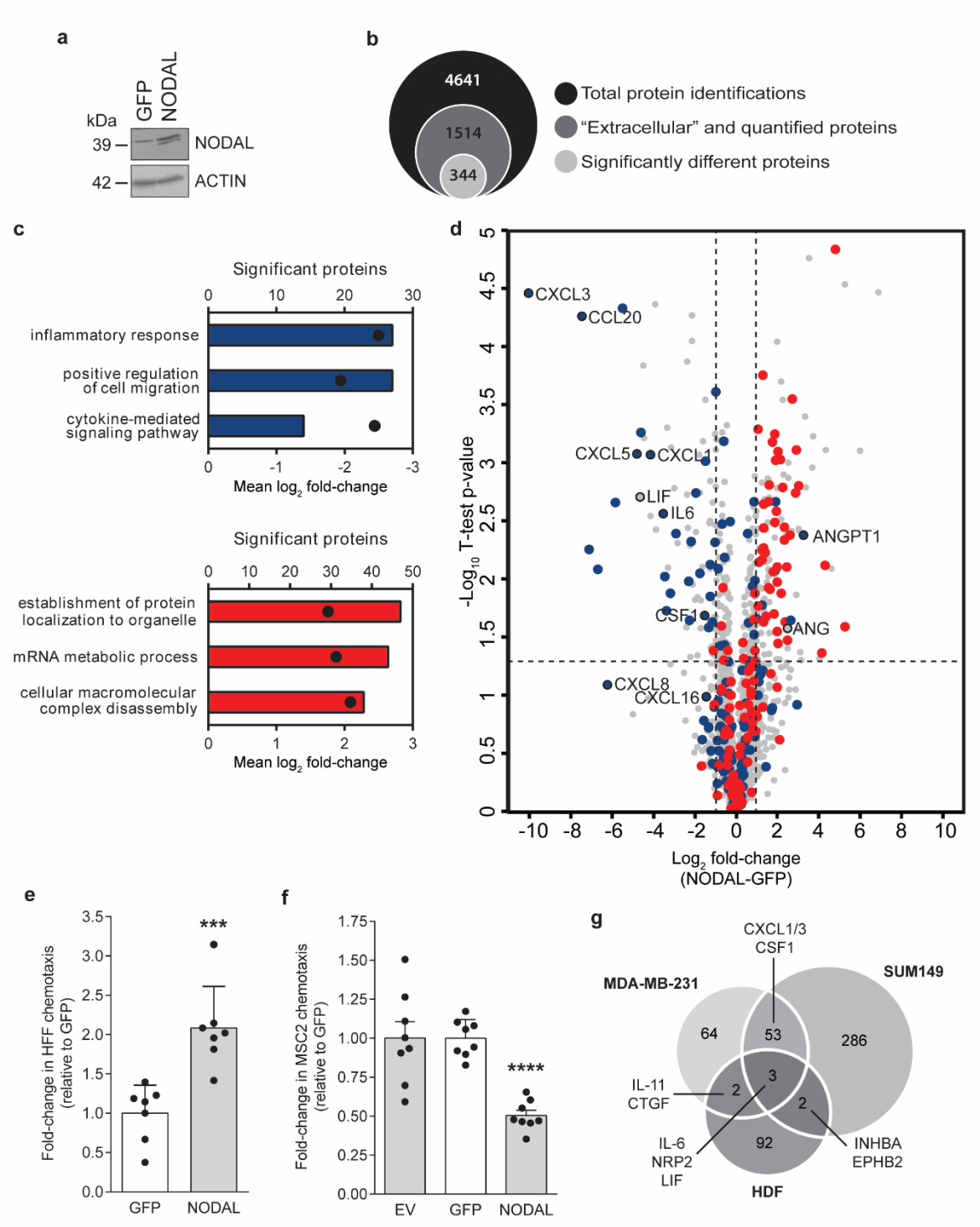

Figure 7. NODAL overexpression alters the SUM149 secretome and affects HFF and MSC chemotaxis. (a) NODAL expression in GFP- or NODAL-overexpressing SUM149 breast cancer cells. Extracellular proteins from serum-free CM (GFP or NODAL) were analyzed by mass spectrometry. **(b)** Venn diagram highlighting total protein identifications, "extracellular" and quantified proteins, and significantly different proteins between GFP and NODAL CM (two-tailed, two sample t-test, $p<0.05$). **(c)** Number of significant proteins (bars) matching to subset of significantly enriched GOBPs (BH FDR threshold<0.02). Mean log_2 fold-changes in GOBPs are indicated by black dots. Blue and red bars highlight GOBPs decreased and increased in SUM149 CM following NODAL overexpression, respectively. **(d)** Volcano plot of quantified "extracellular" proteins. Negative and positive log_2 fold-changes indicate proteins decreased and increased in SUM149 CM following NODAL overexpression, respectively (n=3). All proteins matching to corresponding GOBPs mentioned are highlighted in blue and red. Several cytokines, chemokines and growth factors altered by NODAL are labelled in black. Vertical and horizontal dotted lines indicate log_2 fold-changes ≥2 and the $-log_{10}$ p-value cut-off corresponding to $p<0.05$, respectively. **(e)** NODAL overexpression increased HFF chemotaxis towards CM from SUM149 cells compared to GFP control (n=6); Two-sample t-test, ***$p<0.001$. **(f)** CM from NODAL-overexpressing SUM149 cells decreased MSC chemotaxis compared to empty vector (EV) and GFP controls. Data are presented as mean fold-changes relative to controls from a minimum of three biological replicates ± SD. Black dots indicate replicate values and asterisks indicate significance differences (one-way ANOVA, Dunnett's multiple comparison test) in MSC chemotaxis compared controls (*** $p<0.001$, **** $p<0.0001$). **(g)** Overlap in proteins differentially expressed (increased or decreased) in MDA-MB-231 (shControl versus shNODAL), SUM149 (NODAL versus GFP) and HDF (rhNODAL-treated versus untreated) datasets.

Differential signalling pathways may dictate cell type-dependent effects of NODAL

Our data demonstrate that the effects of NODAL are highly context-dependent. These differential responses may be due, in part, to which signal transduction pathways NODAL induces. Indeed, ELISAs showed that CXCL1 and IL-6 levels were substantially higher in GFP expressing SUM149 cells compared to MDA-MB-231 cell lines grown to similar confluence (**Sup. Fig. 2b, c**), suggesting different regulatory mechanisms between these cell lines. Canonically, NODAL triggers phosphorylation of SMAD2/3 via binding to its receptors ActRIIB/ALK(4/7) and co-receptor CRIPTO[67]. Phospho-SMAD2/3-SMAD4 heterodimers subsequently translocate into the nucleus to regulate the epigenetic status and transcription of target genes. NODAL can also signal

383 non-canonically to activate ERK1/2, which is required for the induction of epithelial-mesenchymal
384 transition (EMT) and invasion[49].

385 Given the disparate effects of NODAL on cytokine secretion in MDA-MB-231 versus SUM149
386 cells, we hypothesized that NODAL may activate different signalling mediators like TGF-β in a
387 cell-type dependent manner[68,69]. Accordingly, the activation of two documented mediators of
388 NODAL signalling (SMAD2/3 and ERK1/2) were measured by western blotting in breast cancer
389 cells wherein NODAL levels had been modified (**Fig. 8**). NODAL knockdown in MDA-MB-231
390 resulted in an expected and previously described reduction in both SMAD2/3 and ERK1/2
391 phosphorylation[49]. While overexpression of NODAL in SUM149 increased SMAD2
392 phosphorylation, a small reduction in ERK1/2 phosphorylation was observed. Moreover,
393 constitutive SMAD2 activation was higher, while ERK1/2 was lower in SUM149 compared to
394 MDA-MB-231 cells. Finally, we examined STAT3 activation, which occurs downstream of IL-6. In
395 accordance with reduced IL-6 levels, NODAL knockdown reduced STAT3 phosphorylation in
396 MDA-MB-231 cells. However, NODAL overexpression did not appear to affect STAT3 activation
397 in SUM149 cells, perhaps due to the highly inflammatory nature of this cell line. These results
398 suggest that some of the observed cell-type-specific effects of NODAL may relate to differential
399 levels of SMAD2/3 and ERK1/2 activation induced by this ligand; MDA-MB-231 cells have higher
400 ERK1/2 and lower SMAD2/3 basal activation compared to SUM149 cells. Hence, NODAL may
401 preferentially signal through SMAD2/3 in SUM149 and ERK1/2 in MDA-MB-231 cells.

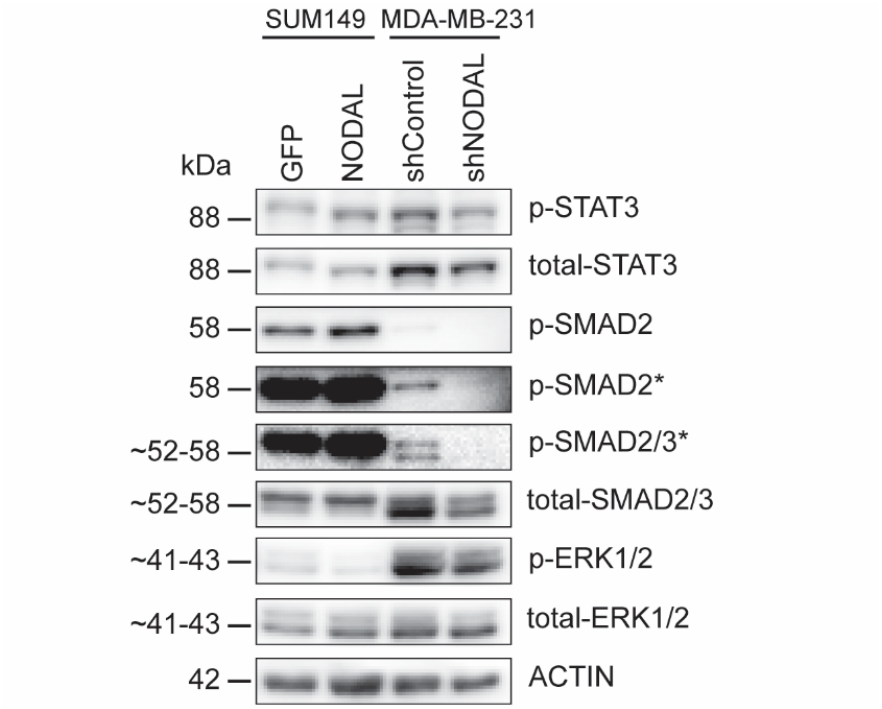

Figure 8. Effects of NODAL manipulation on signalling pathways in MDA-MB-231 and SUM149 cells. Western blotting revealed similarities and differences in activation of downstream pathways. NODAL expression (NODAL and shControl cell lines) was associated with increased phosphorylation of STAT3, SMAD2 and SMAD3. Basal levels of p-SMAD2 and p-ERK1/2 were substantially higher in SUM149 and MDA-MB-231 cell lines, respectively. p-ERK1/2 decreased slightly following NODAL overexpression in SUM149 cells. Western blots are representative images taken from three biological replicates and asterisks denote high contrast image settings.

Discussion

The TME facilitates pro-tumourigenic processes, among which fibroblast activation – a common trait of many cancers, including breast carcinomas[70,71] – plays an important role. Many factors activate fibroblasts, such as TGF-β, CXCL12/SDF-1, PDGFA/B, and IL-6[72-74]. NODAL has been shown to directly induce migration and invasion of breast, pancreatic, and hepatocellular cancer cell lines *in vitro*[43,49,75]. Moreover, ectopic overexpression of NODAL in breast cancer cells indirectly promotes endothelial tube formation by increasing the expression of pro-angiogenic

418 proteins such as PDGFA[45]. Recent efforts have shown that NODAL alters breast cancer cell
419 susceptibility to γδ T cell killing by acting on cancer cells to decrease recognizable antigens on
420 the cell surface. Furthermore, long-term NODAL stimulation reduced Vδ2 T cell antigen receptor
421 expression, suggesting activation of an as-of-yet unidentified signaling pathway in primary γδ T
422 cells[50]. We build upon these studies by showing that NODAL may affect TME function and
423 composition directly or indirectly by broadly regulating the breast cancer secretome. Specifically,
424 we show that NODAL activates fibroblasts directly, but that it affects MSC chemotaxis indirectly,
425 by reprogramming breast cancer cell secretomes.

426 We have shown herein that cells expressing the CAF marker α-SMA are spatially
427 correlated with NODAL-positive cancer cells in human TNBC tissues, and that NODAL expression
428 levels positively correlate to those of stromal α-SMA in these tissues. We demonstrate for the first
429 time that NODAL signals directly on fibroblasts to induce an activated phenotype, characterized
430 by increased proliferation rates, invasive capacity, and the expression of transcripts of known
431 CAF markers. The origin of CAFs has been extensively debated over the years[76-79], with evidence
432 pointing to diverse sources such as resident tissue fibroblasts, bone marrow-derived MSCs,
433 hematopoietic stem cells, epithelial cells that undergo epithelial-mesenchymal transition, and
434 endothelial cells. A recent study has shown that the MDA-MB-231, but not MCF-7, secretome
435 activates MSCs, converting them into tumour-associated MSCs[80]. We similarly show that
436 although MSCs are unable to sense and respond to NODAL signals, they still undergo chemotaxis
437 toward the NODAL-regulated breast cancer cell secretome.

438 Our robust proteomics approach allowed us to uncover dozens of secreted proteins that
439 are affected by NODAL expression in breast cancer cells and may impact MSC recruitment to the
440 breast TME. For these studies, we knocked down NODAL in claudin-low MDA-MB-231 cells that
441 express high basal levels of NODAL, and overexpressed NODAL in SUM149, which represent
442 inflammatory breast cancer cells and express low levels of NODAL. Consistent with the effects of

443 NODAL *in vitro* and *in vivo*, the levels of several pro-angiogenic factors (PDGFA, ANGPT1, and
444 ANG) in breast cancer CM were positively correlated with its expression[45]. However, we also
445 made the seemingly paradoxical discovery that the expression of NODAL in MDA-MB-231 and
446 SUM149 breast cancer cells oppositely regulates cytokines involved in chemotaxis. This
447 difference may be coincident with the models chosen: MDA-MB-231 express relatively low levels
448 of pro-inflammatory cytokines compared to SUM149, and thus the epigenetic regulation of the
449 genes encoding these proteins may vary dramatically between the two cells lines.

450 Our discordant results are not uncommon for studies involving members of the TGF-β
451 family, which function in a context-dependent manner. TGF-β1, for example, induces IL-6
452 production in PC3 and DU145 prostate cancer cells *via* SMAD2/TGFBRII and p38 MAPK[81].
453 Moreover, in MDA-MB-231 and MDA-MB-468 breast cancer cells, TGF-β1 stimulates IL-8
454 (CXCL8) and IL-11 secretion *via* SMAD3/TGFBRI and p38 MAPK[82]. However, in the
455 Polyomavirus middle T antigen transformed mouse mammary carcinoma model, loss of TGF-β
456 signalling results in the upregulation of CXCL1, CXCL5, and CCL20[83]. Remarkably, these factors
457 decreased substantially in SUM149 CM following NODAL overexpression (**Sup. Tables 4 and 6**),
458 thus suggesting negative regulatory roles for both NODAL and TGF-β. We did not observe
459 significant differences in the levels of TGF-β1/2 between breast cancer lines (Sup. Tables 2, 4
460 and 6), hence the effects of NODAL were not likely mediated *via* alterations in TGF-β1/2. Taken
461 together, both NODAL and TGF-β may differentially regulate chemokine and cytokine expression
462 in cancer, depending on the context. This difference should be considered as treatment modalities
463 designed to target these pathways evolve[84].

464 Genes regulated by NODAL appear to be dictated, at least in part, by the accessibility of
465 genomic regions, and NODAL induces histone modifications to affect gene expression[85]. Hence
466 the differential effects of NODAL in MDA-MB-231 versus SUM149 cells may be due to differences
467 in chromatin accessibility in the areas surrounding chemotactic and inflammatory cytokines. The

differences observed may also be due to the ability of NODAL to activate ERK signaling in MDA-MB-231 cells but not in SUM149 cells. Several studies have demonstrated the role of ERK signaling in the upregulation of inflammatory cytokines such as IL-6[86,87]. Hence the effects of NODAL knockdown in MDA-MB-231 cells may be due to reduced ERK signalling.

While IL-6R was detected on MSC, CXCR1 and CXCR2 were not. Heterogeneity in MSC receptor expression has been reported in multiple studies and may be a product of culture conditions and donor heterogeneity[88,89]. For reference, Ponte *et al.* observed CXCR4 and CXCR5 but not CXCR1 or CXCR2 on human BM-MSC[90]. Chamberlain *et al.* also reported high expression for CXCR4 and CXCR5 but low to intermediate expression of CXCR1 and CXCR2, respectively[91]. Conversely, Ringe *et al.* extensively profiled chemokine receptors on human BM-MSC and detected CXCR1 and CXCR2 but noted loss of expression following ten passages[92]. While these pathways may play a role in MSC recruitment to tumours in breast cancer patients, we were unable to test this possibility.

In our hands, MDA-MB-231 cells produced less IL-6 and CXCL1 than those studied by Hartman *et al*., who investigated the role of cytokines in TNBC cell growth[60]. Notwithstanding, neutralizing IL-6 in MDA-MB-231 CM was sufficient to attenuate MSC chemotaxis[29,93,94]. We did not neutralize IL-6 in SUM149 CM; however, CM from either SUM149 or SUM159 breast cancer cells was previously shown to promote migration of aldehyde dehydrogenase-high MSC or macrophage-educated MSC in an IL-6 dependent manner[62,94].

Although CXCR1/2 was not detected on MSC, differences in CXCL1 and CXCL8 levels following NODAL knockdown/overexpression remain important for cancer progression and trafficking of additional cell types and justify additional interrogation. For instance, CXCL1-mediated recruitment of CD11b+Gr1+ myeloid cells enhanced breast cancer cell survival, chemoresistance, and metastasis[61]. Moreover, obesity-associated CXCL1 expression in prostate tumours was linked to adipose-derived stromal cell migration *in vitro* and tumour engraftment *in*

493 *vivo*[95]. Given the importance of NODAL-regulated cytokines in the TME, future studies
494 interrogating the extent to which NODAL may modulate TME composition are warranted.

495 In summary, we demonstrate that NODAL directly activates stromal fibroblasts and that it
496 reshapes the breast cancer secretome, affecting the deposition of factors such as IL-6, which may
497 regulate the recruitment of MSCs, as well as other TME cell types (**Fig. 9**). Expanding our previous
498 discovery that NODAL induces secretion of PDGF and VEGF by breast cancer cells, our present
499 findings illuminate a hitherto unappreciated role for NODAL in the orchestration of the tumour
500 microenvironment.

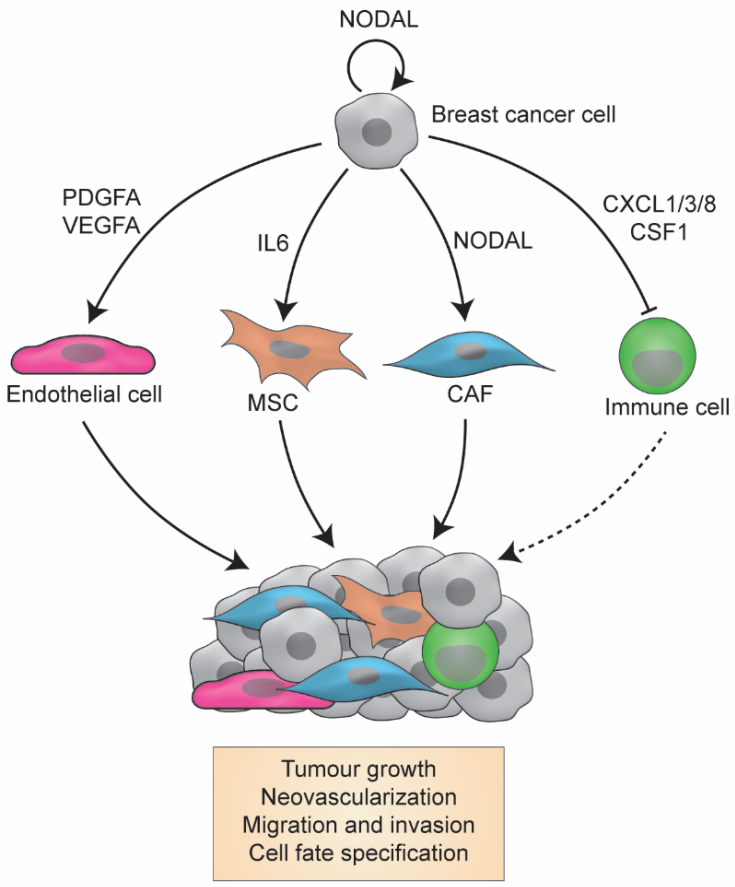

501

502 **Figure 9. Proposed model for NODAL signalling in the breast cancer microenvironment.** NODAL
503 signals directly to breast cancer cells and CAFs, and indirectly regulates secretion of inflammatory,
504 chemotactic and angiogenic factors by breast cancer cells, which act on endothelial and mesenchymal
505 stromal cells and possibly immune cell types. Collectively, NODAL promotes tumorigenic phenotypes
506 including tumour growth, neovascularization, cell migration and cell fate specification.

Materials and Methods

Patients and Tissues

We assessed 41 samples from 20 surgically resected TNBC tumors from cancer patients diagnosed at the Cross Cancer Institute, Edmonton, AB in 2017. This study was carried out in accordance with the recommendations of the Research Ethics Guidelines, Health Research Ethics Board of Alberta – Cancer Committee with written informed consent from all subjects. All subjects gave written informed consent in accordance with the Declaration of Helsinki.

Immunohistochemistry

NODAL and α-SMA staining in TNBC tissues was performed as previously described for NODAL[45]. Briefly, tissue sections were deparaffinized in xylene and hydrated in graded ethanol. Antigen retrieval was performed with citrate buffer pH 6.0, followed by peroxidase and serum-free protein blocking. After incubation with primary antibodies (**Sup. Table 8**), slides were rinsed in TBS-T and treated with Envison+ HRP anti-mouse IgG (Dako, Glostrup, Denmark). Color was produced with 3,3′-Diaminobenzidine (DAB) substrate and counterstained with Mayer's haematoxylin. Samples were dehydrated in graded alcohol and cover slipped with permanent mounting medium.

Evaluation of NODAL and α-SMA staining

Light microscopy and semi-quantitative scoring were performed by two pathologists. The entirety of each slide was assessed. Scores for NODAL were 0, absent; 1, weak or very focal staining; 2, strong but focal or moderate intensity; and 3, strong and extensive staining. The score reflects the intensity of staining observed in the majority of cells. When scored 1-3, NODAL distribution was further identified as focal, diffuse or scattered, and an estimated proportion of tumour cells staining with NODAL was calculated (NODAL percentage in Table I). α-SMA was scored in the

same manner on serial sections from the same cases. Intensity association was measured based on the extent to which α-SMA staining was increased in areas with NODAL-positive cells. Representative images were taken from a Nikon DS U3 camera on Nikon eclipse 80i microscrope (Nikon, Tokyo, Japan) at 400 x (500 px bar = 40 μm).

Cell culture

MDA-MB-231 cells stably expressing scrambled control (shControl) or NODAL targeting (shNODAL) short hairpin RNAs as previously described and validated[45,48,49] were maintained in DMEM/F12 (Gibco, Waltham, MA) supplemented with 10% FBS (Gibco) and 500ng/mL puromycin. To generate SUM149 cells stably expressing an empty vector (EV), green fluorescent protein (GFP) or NODAL, cells were transduced with lentiviral particles (GeneCopoeia, Rockville, MD) overnight then selected and maintained in HAM's F10 (Gibco) supplemented with 10% FBS, 5μg/mL insulin (Santa Cruz Biotechnology, Dallas, TX), 1μg/mL hydrocortisone (Sigma-Aldrich, St. Louis, MO) and 100 ng/mL puromycin. Human BM-MSC lines were maintained in AmnioMAX™ with C100 supplement (Life Technologies, Carlsbad, CA); these lines were previously confirmed to express characteristic stromal markers (>95% CD90+, CD105+, and CD73+) and exhibit multipotent differentiation[56,96]. HFFs (Cascade Biologics, Portland, OR) were maintained in DMEM/F12 supplemented with 10% FBS and HDFs (ATCC, Manassas, VA) in DMEM supplemented with 10% FBS. For SILAC labelling, shControl and shNODAL MDA-MB-231 cells were cultured in DMEM F12 supplemented with dialyzed FBS (Life Technologies) containing light (Advanced ChemTech, Louisville, KY) or heavy (Cambridge Isotope Laboratories, Tewksbury, MA and Silantes GmbH, Germany) isotopes of arginine (0.398mM) and lysine (0.274mM) for at least nine days to achieve >90% label incorporation. SILAC media was additionally supplemented with 400 mg/L of proline (Sigma-Aldrich) to limit arginine to proline conversion[97]. CM was prepared by plating equal cell numbers onto flasks in culture media (Corning, Corning, NY). After 24h (MDA-MB-231 cells) or 48h (SUM149 cells), media was

558 removed, and cells were thoroughly rinsed three times in PBS (with Ca2+ and Mg2+) to remove
559 serum components. Cells were incubated in serum-free media (SFM) with 0.5% BSA for an
560 additional 24h to generate CM (BSA was omitted for LC-MS samples). Conditions used to
561 stimulate cells with rhNODAL and rhIL-6 are specified in the main text.
562
563 **Sample preparation for liquid chromatography-mass spectrometry (LC-MS)**
564 CM (without BSA) were concentrated using 3 kDa molecular weight cut-off (MWCO) Amicon
565 ultracentrifugal units (Millipore, Burlington, MA) and lyophilized overnight. The following day, CM
566 was reconstituted in lysis buffer (8M urea, 50mM ammonium bicarbonate, 10mM dithiothreitol and
567 2% SDS), sonicated (3 X 0.5s pulses) with a probe sonicator (Level 1; Fisher Scientific, Waltham,
568 MA) and quantified using a Pierce™ 660 nm assay (Thermo Fisher Scientific, Waltham, MA) with
569 ionic detergent compatibility reagent. For SILAC samples, light shControl and heavy shNODAL
570 CM were pooled based on equal cell numbers and ~100µg protein were fractionated using SDS-
571 PAGE on 12% acrylamide tris-glycine gels. In-gel digestion with trypsin (1:25 enzyme:protein
572 ratio) was performed on 16-17 slices (fractions) from each lane in biological triplicate as previously
573 described[98]. For label-free samples, ~50µg protein from SUM149 CM were precipitated in
574 chloroform/methanol, digested overnight with trypsin (1:50 ratio) on a water bath shaker and
575 fractionated on SCX StageTips as previously described[98-100]. Peptides were dried in a SpeedVac,
576 reconstituted in 0.1% formic acid (FA; Fisher Scientific) and a volume corresponding to 1/10th of
577 the total material recovered or 1 µg as determined by bicinchoninic acid (BCA) assay (Pierce™,
578 Waltham, MA) was injected for each in-gel and SCX fraction, respectively.
579
580 **LC-MS**
581 In-gel and SCX fractions were analyzed using a Q Exactive or Orbitrap Elite mass spectrometer
582 (Thermo Fisher Scientific), respectively. Samples were injected using a nanoAcquity HPLC
583 system (Waters, Milford, MA) and initially trapped on a Symmetry C18 Trap Column (5 µm, 180

584 µm x 20 mm) for 4 or 5 minutes in 99% Solvent A (Water/0.1% FA)/1% Solvent B
585 (acetonitrile/0.1% FA) at a flow rate of 10 µl/min. Peptides were separated on an ACQUITY
586 Peptide BEH C18 Column (130Å, 1.7µm, 75µm X 250mm) at a flow rate of 300 nL/min maintained
587 at 35°C. The LC-MS gradient for in-gel digests consisted of 1-7% B over 1 minute and 7-37.5%
588 B over 79 minutes. SCX fractions were separated using gradient consisting of 7.5% B over 1
589 minute, 25% B over 179 minutes, 32.5% B over 40 minutes and 60% B over 20 minutes. Column
590 washing and re-equilibration was performed following each run and settings for data acquisition
591 are outlined in **Sup. Table 9**.
592
593 **Data analysis and statistics**
594 Raw MS files were searched in MaxQuant (1.5.2.8) with the Human Uniprot database (reviewed
595 only; updated May 2014 with 40,550 entries)[101]. Missed cleavages were set to 3 and I=L. Cysteine
596 carbamidomethylation was set as a fixed modification. Oxidation (M), n-terminal acetylation
597 (protein), and deamidation (NQ) were used as variable modifications (max. number of
598 modifications per peptide = 5) and min ratio count was set to 1. All other settings were left at
599 default. The match-between-runs feature was utilized to maximize proteome coverage and
600 quantitation between samples. Datasets were loaded into Perseus[59] (version 1.5.5.3) and proteins
601 identified by site, reverse and potential contaminants were removed[59]. Protein identifications with
602 quantitative values in ≥2 biological replicates were retained for downstream analysis unless
603 specified elsewhere. Missing values were imputed using a width of 0.3 and down shift of 1.8 for
604 label free datasets. Statistical analysis was performed in Perseus or GraphPad Prism version
605 6.01 (San Diego, CA). All experiments were carried in at least three biological replicates unless
606 specified otherwise. Where specified, replicate treatment values were normalised to the control
607 group and relative fold-changes were reported. Two-tailed, one sample and two-sample t-tests
608 ($p<0.05$) were performed to determine statistical differences unless more than two conditions

were being compared and a one-way ANOVA using Dunnett's multiple comparison test ($p<0.05$) was performed instead.

Chemotaxis and invasion assays

MSCs were rinsed in warm PBS (with Ca2+ and Mg2+) and serum starved for ~2h in AmnioMAX™ prior to dissociation with trypsin for chemotaxis assays. In parallel, 8μM transwells (Falcon®, Corning, NY) were coated with 10μg/cm^2 of bovine fibronectin (Sigma-Aldrich) in 100μL of PBS for 2h. After coating, excess solution was aspirated and 40K MSCs in 0.5mL of DMEM F12+0.5% BSA were plated in each transwell. HFFs were serum starved 24h prior to dissociation and plated at a density of 50K cells/transwell. For HFF chemotaxis and invasion assays, fibronectin and Matrigel™ (Corning) were omitted and included, respectively. To the bottom chamber, 1mL of DMEM/F12 + 0.5% BSA or CM was added +/- rhNODAL (R&D Systems, Minneapolis, MN), rhIL-6 (eBioscience, San Diego, CA), isotype or IL-6 neutralizing monoclonal antibodies (R&D Systems). After ~24h, transwells were rinsed in warm PBS and placed in cold methanol for 20 minutes to fix migrating cells. After fixing, transwells were rinsed in PBS and the inside membrane was thoroughly wiped with a cotton swab to remove non-migrated cells. Membranes were excised and mounted onto glass slides with ProLong™ Gold Antifade Mountant with DAPI (Invitrogen, Carlsbad, CA). Migrated cells were counted from at least 5-10 high power fields uniformly distributed across the entire membrane for each condition.

Western blotting

Cells were thoroughly washed with PBS (with Ca2+ and Mg2+) and directly lysed on tissue culture plates in lysis buffer. Lysates recovered by pipetting were sonicated with a probe sonicator (20 X 0.5s pulses) to shear DNA and reduce viscosity. Equal protein amounts (15-25μg) were separated on hand cast 8-20% acrylamide Tris-glycine gels then transferred to Immobilon-P® PVDF membranes (Millipore). Membranes were stained with amido black and rinsed in ddH_2O for 5

minutes followed by blocking for 1h on rocker in 5% non-fat dry milk in TBST (Tris-buffered saline, 0.1% Tween 20) and overnight incubation in primary antibody at 4°C. Chemiluminescent detection was performed using film or a VersaDoc CCD camera with Clarity™ Western ECL Substrate and horseradish peroxidase-conjugated secondary antibodies (Bio-Rad, Hercules, CA) the next day. Antibody information is available in **Sup. Table 8**. Actin and Tubulin were used as loading controls. PVDF membranes were stippled in 0.2 M NaOH and re-probed when possible, otherwise western blots were run in duplicate.

Real-time PCR

RNA was isolated from cells and treated with DNAse using a PerfectPure RNA cultured cell kit (5PRIME). RNA was quantified by NanoDrop™ (Thermo Fisher Scientific) and 2µg was reverse transcribed with a High Capacity cDNA Reverse Transcription kit (Applied Biosystems, Foster City, CA). Real-time PCR was performed with TaqMan™ Universal PCR Master Mix (Applied Biosystems) on a Bio-Rad CFX96/384 thermocycler. *HPRT1* or *RPLPO* were used as housekeeping genes to monitor variations between biological replicates. TaqMan™ primer probes were purchased from Applied Biosystems and are listed in **Sup. Table 10**.

Flow cytometry

MSCs dissociated in 10mM EDTA/PBS solution for 5-10 minutes were resuspended in 5% FBS/PBS, counted, and pelleted at 450xg. Excess buffer was aspirated and MSCs were divided into 50-100K cell aliquots in 100µL of 5% FBS/PBS. Isotype controls and primary antibodies (**Sup. Table 8**) were added to cell suspensions and incubated for ~45 minutes in the dark on ice. Cell suspensions were washed in excess 5% FBS/PBS and pelleted to remove unbound antibody. Flow cytometry data was acquired on an LSR II (Becton Dickinson, Franklin Lakes, NJ) using FACSDiva (Becton Dickinson) at the London Regional Flow Cytometry Facility and analyzed with FlowJo (FlowJo LLC, Ashland, OR, Version 10.0.8r1). The gating strategy for live singlets was

based on forward and side-scatter and is illustrated in **Sup. Fig. 5**. The CellTrace™ Violet Cell Proliferation assay (Thermo Fisher Scientific) was performed as instructed by the manufacturer. Briefly, MSCs were labelled in suspension with CellTrace™ Violet dye. After 20 min incubation at 37°C in the dark, MSCs were incubated for 5 min with culture medium to remove any free dye remaining in the solution. MSCs were pelleted, resuspended in fresh pre-warmed complete culture medium, and plated onto 6-well plates prior to incubation with CM.

ELISAs

ELISA kits were purchased from eBioscience (IL-6) or R&D Systems (CXCL1, CXCL8 and CSF1) and performed according to the manufacturer's specifications using CM derived from MDA-MB-231 and SUM149 cell lines.

Gene expression profiling

HDFs were cultured until ~40-60% confluence, washed twice with PBS and incubated overnight in DMEM+0.5%FBS. The following day, cells were treated +/- rhNODAL (10 ng/mL) for 6h and RNA was harvested using TRIzol™ (Invitrogen). RNA was subjected to expression profiling at the London Regional Genomics Centre essentially as previously described[102,103]. RNA quality was assessed using an Agilent 2100 Bioanalyzer (Agilent Technologies, Santa Clara, CA) prior to preparing single stranded complimentary DNA (sscDNA) from 200ng of total RNA (Ambion WT Expression Kit for Affymetrix GeneChip Whole Transcript WT Expression Arrays; Applied Biosystems, Carlsbad, CA) according to the Affymetrix User Manual (Affymetrix, Santa Clara, CA). In total, 5.5µg of sscDNA was synthesized, converted into cRNA, end labeled and hybridized (16h at 45°C) to Human Gene 1.0 ST arrays. Liquid handling steps were performed by a GeneChip Fluidics Station 450 and GeneChips were scanned (GeneChip Scanner 3000 7G; Affymetrix) using Command Console v1.1 to generate Probe level (.CEL file) data. Gene level data was generated using the RMA algorithm[104]. Partek Genomics Suite v6.5 (St. Louis, MO) was

used to determine gene level ANOVA p-values and fold-changes. Fold-changes were obtained by averaging data from two experiments (GeneSpring, Agilent). Fold-changes exceeding 1.7 in response to rhNODAL were required to identify a transcript as being altered ($p<0.05$). Altered genes were annotated using DAVID (version 6.7) and lists enriched >3.5 fold and comprised of >10 genes were reported.

Acknowledgements

We thank Dr. Dean Betts (Western University), Dr. John Di Guglielmo (Western University) and Dr. Dwayne Jackson (Western University) for providing access to PCR and imaging equipment and Paula Pittock for technical support. The work was funded by operating grants from the CIHR and the Canadian Breast Cancer Foundation awarded to LMP.

Competing Interests

None of the authors has competing interests to declare.

References

1. Martinez-Outschoorn UE, Goldberg A, Lin Z, Ko YH, Flomenberg N, Wang C, Pavlides S, Pestell RG, Howell A, Sotgia F, Lisanti MP. Anti-estrogen resistance in breast cancer is induced by the tumor microenvironment and can be overcome by inhibiting mitochondrial function in epithelial cancer cells. *Cancer Biol Ther.* 2011;12(10):924-938.
2. Farmer P, Bonnefoi H, Anderle P, Cameron D, Wirapati P, Becette V, Andre S, Piccart M, Campone M, Brain E, Macgrogan G, Petit T, Jassem J, Bibeau F, Blot E, Bogaerts J, Aguet M, Bergh J, Iggo R, Delorenzi M. A stroma-related gene signature predicts resistance to neoadjuvant chemotherapy in breast cancer. *Nat Med.* 2009;15(1):68-74.
3. Dittmer J, Leyh B. The impact of tumor stroma on drug response in breast cancer. *Semin Cancer Biol.* 2015;31:3-15.
4. Allinen M, Beroukhim R, Cai L, Brennan C, Lahti-Domenici J, Huang H, Porter D, Hu M, Chin L, Richardson A, Schnitt S, Sellers WR, Polyak K. Molecular characterization of the tumor microenvironment in breast cancer. *Cancer Cell.* 2004;6(1):17-32.
5. Ma XJ, Dahiya S, Richardson E, Erlander M, Sgroi DC. Gene expression profiling of the tumor microenvironment during breast cancer progression. *Breast Cancer Res.* 2009;11(1):R7.
6. Su S, Chen J, Yao H, Liu J, Yu S, Lao L, Wang M, Luo M, Xing Y, Chen F, Huang D, Zhao J, Yang L, Liao D, Su F, Li M, Liu Q, Song E. CD10(+)GPR77(+) Cancer-Associated Fibroblasts Promote Cancer Formation and Chemoresistance by Sustaining Cancer Stemness. *Cell.* 2018;172(4):841-856.e816.
7. Chatterjee S, Bhat V, Berdnikov A, Liu J, Zhang G, Buchel E, Safneck J, Marshall AJ, Murphy LC, Postovit LM, Raouf A. Paracrine Crosstalk between Fibroblasts and ER(+) Breast Cancer Cells Creates an IL1beta-Enriched Niche that Promotes Tumor Growth. *iScience.* 2019;19:388-401.
8. Kalluri R. The biology and function of fibroblasts in cancer. *Nat Rev Cancer.* 2016;16(9):582-598.
9. Gabbiani G. The myofibroblast in wound healing and fibrocontractive diseases. *J Pathol.* 2003;200(4):500-503.
10. Rockey DC, Weymouth N, Shi Z. Smooth muscle alpha actin (Acta2) and myofibroblast function during hepatic wound healing. *PLoS One.* 2013;8(10):e77166.
11. Fukumura D, Xavier R, Sugiura T, Chen Y, Park EC, Lu N, Selig M, Nielsen G, Taksir T, Jain RK, Seed B. Tumor induction of VEGF promoter activity in stromal cells. *Cell.* 1998;94(6):715-725.
12. Buechler MB, Turley SJ. A short field guide to fibroblast function in immunity. *Semin Immunol.* 2018;35:48-58.
13. Biffi G, Oni TE, Spielman B, Hao Y, Elyada E, Park Y, Preall J, Tuveson DA. IL1-Induced JAK/STAT Signaling Is Antagonized by TGFbeta to Shape CAF Heterogeneity in Pancreatic Ductal Adenocarcinoma. *Cancer Discov.* 2019;9(2):282-301.
14. Brizzi MF, Tarone G, Defilippi P. Extracellular matrix, integrins, and growth factors as tailors of the stem cell niche. *Curr Opin Cell Biol.* 2012;24(5):645-651.
15. Le Guen L, Marchal S, Faure S, de Santa Barbara P. Mesenchymal-epithelial interactions during digestive tract development and epithelial stem cell regeneration. *Cell Mol Life Sci.* 2015;72(20):3883-3896.
16. De Wever O, Nguyen QD, Van Hoorde L, Bracke M, Bruyneel E, Gespach C, Mareel M. Tenascin-C and SF/HGF produced by myofibroblasts in vitro provide convergent pro-invasive signals to human colon cancer cells through RhoA and Rac. *FASEB J.* 2004;18(9):1016-1018.
17. Tomasek JJ, Gabbiani G, Hinz B, Chaponnier C, Brown RA. Myofibroblasts and mechano-regulation of connective tissue remodelling. *Nat Rev Mol Cell Biol.* 2002;3(5):349-363.
18. Erez N, Truitt M, Olson P, Arron ST, Hanahan D. Cancer-Associated Fibroblasts Are Activated in Incipient Neoplasia to Orchestrate Tumor-Promoting Inflammation in an NF-kappaB-Dependent Manner. *Cancer Cell.* 2010;17(2):135-147.
19. Calvo F, Ranftl R, Hooper S, Farrugia AJ, Moeendarbary E, Bruckbauer A, Batista F, Charras G, Sahai E. Cdc42EP3/BORG2 and Septin Network Enables Mechano-transduction and the Emergence of Cancer-Associated Fibroblasts. *Cell Rep.* 2015;13(12):2699-2714.
20. Amatangelo MD, Bassi DE, Klein-Szanto AJ, Cukierman E. Stroma-derived three-dimensional matrices are necessary and sufficient to promote desmoplastic differentiation of normal fibroblasts. *Am J Pathol.* 2005;167(2):475-488.

21. Orimo A, Gupta PB, Sgroi DC, Arenzana-Seisdedos F, Delaunay T, Naeem R, Carey VJ, Richardson AL, Weinberg RA. Stromal fibroblasts present in invasive human breast carcinomas promote tumor growth and angiogenesis through elevated SDF-1/CXCL12 secretion. *Cell.* 2005;121(3):335-348.
22. Heo TH, Wahler J, Suh N. Potential therapeutic implications of IL-6/IL-6R/gp130-targeting agents in breast cancer. *Oncotarget.* 2016;7(13):15460-15473.
23. Bartoschek M, Oskolkov N, Bocci M, Lovrot J, Larsson C, Sommarin M, Madsen CD, Lindgren D, Pekar G, Karlsson G, Ringner M, Bergh J, Bjorklund A, Pietras K. Spatially and functionally distinct subclasses of breast cancer-associated fibroblasts revealed by single cell RNA sequencing. *Nat Commun.* 2018;9(1):5150.
24. Direkze NC, Jeffery R, Hodivala-Dilke K, Hunt T, Playford RJ, Elia G, Poulsom R, Wright NA, Alison MR. Bone marrow-derived stromal cells express lineage-related messenger RNA species. *Cancer Res.* 2006;66(3):1265-1269.
25. Worthley DL, Ruszkiewicz A, Davies R, Moore S, Nivison-Smith I, Bik To L, Browett P, Western R, Durrant S, So J, Young GP, Mullighan CG, Bardy PG, Michael MZ. Human gastrointestinal neoplasia-associated myofibroblasts can develop from bone marrow-derived cells following allogeneic stem cell transplantation. *Stem Cells.* 2009;27(6):1463-1468.
26. Quante M, Tu SP, Tomita H, Gonda T, Wang SS, Takashi S, Baik GH, Shibata W, Diprete B, Betz KS, Friedman R, Varro A, Tycko B, Wang TC. Bone marrow-derived myofibroblasts contribute to the mesenchymal stem cell niche and promote tumor growth. *Cancer Cell.* 2011;19(2):257-272.
27. Goldstein RH, Reagan MR, Anderson K, Kaplan DL, Rosenblatt M. Human bone marrow-derived MSCs can home to orthotopic breast cancer tumors and promote bone metastasis. *Cancer Res.* 2010;70(24):10044-10050.
28. Mishra PJ, Mishra PJ, Humeniuk R, Medina DJ, Alexe G, Mesirov JP, Ganesan S, Glod JW, Banerjee D. Carcinoma-associated fibroblast-like differentiation of human mesenchymal stem cells. *Cancer Res.* 2008;68(11):4331-4339.
29. Shangguan L, Ti X, Krause U, Hai B, Zhao Y, Yang Z, Liu F. Inhibition of TGF-beta/Smad signaling by BAMBI blocks differentiation of human mesenchymal stem cells to carcinoma-associated fibroblasts and abolishes their protumor effects. *Stem Cells.* 2012;30(12):2810-2819.
30. Spaeth E, Klopp A, Dembinski J, Andreeff M, Marini F. Inflammation and tumor microenvironments: defining the migratory itinerary of mesenchymal stem cells. *Gene Ther.* 2008;15(10):730-738.
31. Pelham RJ, Rodgers L, Hall I, Lucito R, Nguyen KC, Navin N, Hicks J, Mu D, Powers S, Wigler M, Botstein D. Identification of alterations in DNA copy number in host stromal cells during tumor progression. *Proc Natl Acad Sci U S A.* 2006;103(52):19848-19853.
32. Patocs A, Zhang L, Xu Y, Weber F, Caldes T, Mutter GL, Platzer P, Eng C. Breast-cancer stromal cells with TP53 mutations and nodal metastases. *N Engl J Med.* 2007;357(25):2543-2551.
33. Rummel S, Valente AL, Kane JL, Shriver CD, Ellsworth RE. Genomic (in)stability of the breast tumor microenvironment. *Mol Cancer Res.* 2012;10(12):1526-1531.
34. Qiu W, Hu M, Sridhar A, Opeskin K, Fox S, Shipitsin M, Trivett M, Thompson ER, Ramakrishna M, Gorringe KL, Polyak K, Haviv I, Campbell IG. No evidence of clonal somatic genetic alterations in cancer-associated fibroblasts from human breast and ovarian carcinomas. *Nat Genet.* 2008;40(5):650-655.
35. Fiegl H, Millinger S, Goebel G, Muller-Holzner E, Marth C, Laird PW, Widschwendter M. Breast cancer DNA methylation profiles in cancer cells and tumor stroma: association with HER-2/neu status in primary breast cancer. *Cancer Res.* 2006;66(1):29-33.
36. Hu M, Yao J, Cai L, Bachman KE, van den Brule F, Velculescu V, Polyak K. Distinct epigenetic changes in the stromal cells of breast cancers. *Nat Genet.* 2005;37(8):899-905.
37. Tyan SW, Hsu CH, Peng KL, Chen CC, Kuo WH, Lee EY, Shew JY, Chang KJ, Juan LJ, Lee WH. Breast cancer cells induce stromal fibroblasts to secrete ADAMTS1 for cancer invasion through an epigenetic change. *PLoS One.* 2012;7(4):e35128.
38. Patel S, Ngounou Wetie AG, Darie CC, Clarkson BD. Cancer secretomes and their place in supplementing other hallmarks of cancer. *Adv Exp Med Biol.* 2014;806:409-442.
39. da Cunha BR, Domingos C, Stefanini ACB, Henrique T, Polachini GM, Castelo-Branco P, Tajara EH. Cellular Interactions in the Tumor Microenvironment: The Role of Secretome. *J Cancer.* 2019;10(19):4574-4587.

40. Madden EC, Gorman AM, Logue SE, Samali A. Tumour Cell Secretome in Chemoresistance and Tumour Recurrence. *Trends Cancer.* 2020;6(6):489-505.
41. Topczewska JM, Postovit LM, Margaryan NV, Sam A, Hess AR, Wheaton WW, Nickoloff BJ, Topczewski J, Hendrix MJ. Embryonic and tumorigenic pathways converge via Nodal signaling: role in melanoma aggressiveness. *Nat Med.* 2006;12(8):925-932.
42. Quail DF, Siegers GM, Jewer M, Postovit LM. Nodal signalling in embryogenesis and tumourigenesis. *Int J Biochem Cell Biol.* 2013;45(4):885-898.
43. Chen J, Liu WB, Jia WD, Xu GL, Ma JL, Ren Y, Chen H, Sun SN, Huang M, Li JS. Embryonic morphogen nodal is associated with progression and poor prognosis of hepatocellular carcinoma. *PLoS One.* 2014;9(1):e85840.
44. Strizzi L, Hardy KM, Margaryan NV, Hillman DW, Seftor EA, Chen B, Geiger XJ, Thompson EA, Lingle WL, Andorfer CA, Perez EA, Hendrix MJ. Potential for the embryonic morphogen Nodal as a prognostic and predictive biomarker in breast cancer. *Breast Cancer Res.* 2012;14(3):R75.
45. Quail DF, Walsh LA, Zhang G, Findlay SD, Moreno J, Fung L, Ablack A, Lewis JD, Done SJ, Hess DA, Postovit LM. Embryonic protein nodal promotes breast cancer vascularization. *Cancer Res.* 2012;72(15):3851-3863.
46. Guo Q, Li VZ, Nichol JN, Huang F, Yang W, Preston SEJ, Talat Z, Lefrere H, Yu H, Zhang G, Basik M, Goncalves C, Zhan Y, Plourde D, Su J, Torres J, Marques M, Habyan SA, Bijian K, Amant F, Witcher M, Behbod F, McCaffrey L, Alaoui-Jamali M, Giannakopoulos NV, Brackstone M, Postovit LM, Del Rincon SV, Miller WH, Jr. MNK1/NODAL Signaling Promotes Invasive Progression of Breast Ductal Carcinoma In Situ. *Cancer Res.* 2019;79(7):1646-1657.
47. Jewer M, Lee L, Leibovitch M, Zhang G, Liu J, Findlay SD, Vincent KM, Tandoc K, Dieters-Castator D, Quail DF, Dutta I, Coatham M, Xu Z, Puri A, Guan BJ, Hatzoglou M, Brumwell A, Uniacke J, Patsis C, Koromilas A, Schueler J, Siegers GM, Topisirovic I, Postovit LM. Translational control of breast cancer plasticity. *Nat Commun.* 2020;11(1):2498.
48. Quail DF, Zhang G, Walsh LA, Siegers GM, Dieters-Castator DZ, Findlay SD, Broughton H, Putman DM, Hess DA, Postovit LM. Embryonic morphogen nodal promotes breast cancer growth and progression. *PLoS One.* 2012;7(11):e48237.
49. Quail DF, Zhang G, Findlay SD, Hess DA, Postovit LM. Nodal promotes invasive phenotypes via a mitogen-activated protein kinase-dependent pathway. *Oncogene.* 2014;33(4):461-473.
50. Siegers GM, Dutta I, Kang EY, Huang J, Köbel M, Postovit L-M. Aberrantly Expressed Embryonic Protein NODAL Alters Breast Cancer Cell Susceptibility to γδ T Cell Cytotoxicity. *Frontiers in Immunology.* 2020;11(1287).
51. Pang T, Yin X, Luo T, Lu Z, Nie M, Yin K, Xue X. Cancer-associated fibroblasts promote malignancy of gastric cancer cells via Nodal signalling. *Cell Biochem Funct.* 2020;38(1):4-11.
52. Li Z, Zhang J, Zhou J, Lu L, Wang H, Zhang G, Wan G, Cai S, Du J. Nodal Facilitates Differentiation of Fibroblasts to Cancer-Associated Fibroblasts that Support Tumor Growth in Melanoma and Colorectal Cancer. *Cells.* 2019;8(6).
53. Huang da W, Sherman BT, Lempicki RA. Systematic and integrative analysis of large gene lists using DAVID bioinformatics resources. *Nat Protoc.* 2009;4(1):44-57.
54. Ali HR, Jackson HW, Zanotelli VRT, Danenberg E, Fischer JR, Bardwell H, Provenzano E, CRUK IMAXT Grand Challenge Team, Rueda OM, Chin SF, Aparicio S, Caldas C, Bodenmiller B. Imaging mass cytometry and multiplatform genomics define the phenogenomic landscape of breast cancer. *Nature Cancer.* 2020;1(2):163–175.
55. Capoccia BJ, Robson DL, Levac KD, Maxwell DJ, Hohm SA, Neelamkavil MJ, Bell GI, Xenocostas A, Link DC, Piwnica-Worms D, Nolta JA, Hess DA. Revascularization of ischemic limbs after transplantation of human bone marrow cells with high aldehyde dehydrogenase activity. *Blood.* 2009;113(21):5340-5351.
56. Bell GI, Broughton HC, Levac KD, Allan DA, Xenocostas A, Hess DA. Transplanted human bone marrow progenitor subtypes stimulate endogenous islet regeneration and revascularization. *Stem Cells Dev.* 2012;21(1):97-109.
57. Geiger T, Wehner A, Schaab C, Cox J, Mann M. Comparative proteomic analysis of eleven common cell lines reveals ubiquitous but varying expression of most proteins. *Mol Cell Proteomics.* 2012;11(3):M111 014050.

58. Pozniak Y, Balint-Lahat N, Rudolph JD, Lindskog C, Katzir R, Avivi C, Ponten F, Ruppin E, Barshack I, Geiger T. System-wide Clinical Proteomics of Breast Cancer Reveals Global Remodeling of Tissue Homeostasis. *Cell Syst.* 2016;2(3):172-184.
59. Tyanova S, Temu T, Sinitcyn P, Carlson A, Hein MY, Geiger T, Mann M, Cox J. The Perseus computational platform for comprehensive analysis of (prote)omics data. *Nat Methods.* 2016;13(9):731-740.
60. Hartman ZC, Poage GM, den Hollander P, Tsimelzon A, Hill J, Panupinthu N, Zhang Y, Mazumdar A, Hilsenbeck SG, Mills GB, Brown PH. Growth of triple-negative breast cancer cells relies upon coordinate autocrine expression of the proinflammatory cytokines IL-6 and IL-8. *Cancer Res.* 2013;73(11):3470-3480.
61. Acharyya S, Oskarsson T, Vanharanta S, Malladi S, Kim J, Morris PG, Manova-Todorova K, Leversha M, Hogg N, Seshan VE, Norton L, Brogi E, Massague J. A CXCL1 paracrine network links cancer chemoresistance and metastasis. *Cell.* 2012;150(1):165-178.
62. Liu S, Ginestier C, Ou SJ, Clouthier SG, Patel SH, Monville F, Korkaya H, Heath A, Dutcher J, Kleer CG, Jung Y, Dontu G, Taichman R, Wicha MS. Breast cancer stem cells are regulated by mesenchymal stem cells through cytokine networks. *Cancer Res.* 2011;71(2):614-624.
63. Bertero A, Madrigal P, Galli A, Hubner NC, Moreno I, Burks D, Brown S, Pedersen RA, Gaffney D, Mendjan S, Pauklin S, Vallier L. Activin/nodal signaling and NANOG orchestrate human embryonic stem cell fate decisions by controlling the H3K4me3 chromatin mark. *Genes Dev.* 2015;29(7):702-717.
64. Lim B, Woodward WA, Wang X, Reuben JM, Ueno NT. Inflammatory breast cancer biology: the tumour microenvironment is key. *Nat Rev Cancer.* 2018;18(8):485-499.
65. Kishimoto K, Liu S, Tsuji T, Olson KA, Hu GF. Endogenous angiogenin in endothelial cells is a general requirement for cell proliferation and angiogenesis. *Oncogene.* 2005;24(3):445-456.
66. Fagiani E, Christofori G. Angiopoietins in angiogenesis. *Cancer Lett.* 2013;328(1):18-26.
67. Massague J. TGFbeta signalling in context. *Nat Rev Mol Cell Biol.* 2012;13(10):616-630.
68. Zhang Y, Alexander PB, Wang XF. TGF-beta Family Signaling in the Control of Cell Proliferation and Survival. *Cold Spring Harb Perspect Biol.* 2017;9(4).
69. Derynck R, Zhang YE. Smad-dependent and Smad-independent pathways in TGF-beta family signalling. *Nature.* 2003;425(6958):577-584.
70. Buchsbaum RJ, Oh SY. Breast Cancer-Associated Fibroblasts: Where We Are and Where We Need to Go. *Cancers (Basel).* 2016;8(2).
71. Marsh T, Pietras K, McAllister SS. Fibroblasts as architects of cancer pathogenesis. *Biochim Biophys Acta.* 2013;1832(7):1070-1078.
72. Shao ZM, Nguyen M, Barsky SH. Human breast carcinoma desmoplasia is PDGF initiated. *Oncogene.* 2000;19(38):4337-4345.
73. Hugo HJ, Lebret S, Tomaskovic-Crook E, Ahmed N, Blick T, Newgreen DF, Thompson EW, Ackland ML. Contribution of Fibroblast and Mast Cell (Afferent) and Tumor (Efferent) IL-6 Effects within the Tumor Microenvironment. *Cancer Microenviron.* 2012;5(1):83-93.
74. Kojima Y, Acar A, Eaton EN, Mellody KT, Scheel C, Ben-Porath I, Onder TT, Wang ZC, Richardson AL, Weinberg RA, Orimo A. Autocrine TGF-beta and stromal cell-derived factor-1 (SDF-1) signaling drives the evolution of tumor-promoting mammary stromal myofibroblasts. *Proc Natl Acad Sci U S A.* 2010;107(46):20009-20014.
75. Duan W, Li R, Ma J, Lei J, Xu Q, Jiang Z, Nan L, Li X, Wang Z, Huo X, Han L, Wu Z, Wu E, Ma Q. Overexpression of Nodal induces a metastatic phenotype in pancreatic cancer cells via the Smad2/3 pathway. *Oncotarget.* 2015;6(3):1490-1506.
76. LeBleu VS, Kalluri R. A peek into cancer-associated fibroblasts: origins, functions and translational impact. *Dis Model Mech.* 2018;11(4).
77. Shiga K, Hara M, Nagasaki T, Sato T, Takahashi H, Takeyama H. Cancer-Associated Fibroblasts: Their Characteristics and Their Roles in Tumor Growth. *Cancers (Basel).* 2015;7(4):2443-2458.
78. Orimo A, Weinberg RA. Heterogeneity of stromal fibroblasts in tumors. *Cancer Biol Ther.* 2007;6(4):618-619.
79. Sugimoto H, Mundel TM, Kieran MW, Kalluri R. Identification of fibroblast heterogeneity in the tumor microenvironment. *Cancer Biol Ther.* 2006;5(12):1640-1646.

80. Blache U, Horton ER, Xia T, Schoof EM, Blicher LH, Schonenberger A, Snedeker JG, Martin I, Erler JT, Ehrbar M. Mesenchymal stromal cell activation by breast cancer secretomes in bioengineered 3D microenvironments. *Life Sci Alliance.* 2019;2(3).
81. Park JI, Lee MG, Cho K, Park BJ, Chae KS, Byun DS, Ryu BK, Park YK, Chi SG. Transforming growth factor-beta1 activates interleukin-6 expression in prostate cancer cells through the synergistic collaboration of the Smad2, p38-NF-kappaB, JNK, and Ras signaling pathways. *Oncogene.* 2003;22(28):4314-4332.
82. Gupta J, Robbins J, Jilling T, Seth P. TGFbeta-dependent induction of interleukin-11 and interleukin-8 involves SMAD and p38 MAPK pathways in breast tumor models with varied bone metastases potential. *Cancer Biol Ther.* 2011;11(3):311-316.
83. Bierie B, Chung CH, Parker JS, Stover DG, Cheng N, Chytil A, Aakre M, Shyr Y, Moses HL. Abrogation of TGF-beta signaling enhances chemokine production and correlates with prognosis in human breast cancer. *J Clin Invest.* 2009;119(6):1571-1582.
84. Hendrix MJ, Kandela I, Mazar AP, Seftor EA, Seftor RE, Margaryan NV, Strizzi L, Murphy GF, Long GV, Scolyer RA. Targeting melanoma with front-line therapy does not abrogate Nodal-expressing tumor cells. *Lab Invest.* 2017;97(2):176-186.
85. Coda DM, Gaarenstroom T, East P, Patel H, Miller DS, Lobley A, Matthews N, Stewart A, Hill CS. Distinct modes of SMAD2 chromatin binding and remodeling shape the transcriptional response to NODAL/Activin signaling. *Elife.* 2017;6.
86. Yun MR, Choi HM, Kang HN, Lee Y, Joo HS, Kim DH, Kim HR, Hong MH, Yoon SO, Cho BC. ERK-dependent IL-6 autocrine signaling mediates adaptive resistance to pan-PI3K inhibitor BKM120 in head and neck squamous cell carcinoma. *Oncogene.* 2018;37(3):377-388.
87. Balko JM, Schwarz LJ, Bhola NE, Kurupi R, Owens P, Miller TW, Gomez H, Cook RS, Arteaga CL. Activation of MAPK pathways due to DUSP4 loss promotes cancer stem cell-like phenotypes in basal-like breast cancer. *Cancer Res.* 2013;73(20):6346-6358.
88. Karp JM, Leng Teo GS. Mesenchymal stem cell homing: the devil is in the details. *Cell Stem Cell.* 2009;4(3):206-216.
89. Dominici M, Le Blanc K, Mueller I, Slaper-Cortenbach I, Marini F, Krause D, Deans R, Keating A, Prockop D, Horwitz E. Minimal criteria for defining multipotent mesenchymal stromal cells. The International Society for Cellular Therapy position statement. *Cytotherapy.* 2006;8(4):315-317.
90. Ponte AL, Marais E, Gallay N, Langonne A, Delorme B, Herault O, Charbord P, Domenech J. The in vitro migration capacity of human bone marrow mesenchymal stem cells: comparison of chemokine and growth factor chemotactic activities. *Stem Cells.* 2007;25(7):1737-1745.
91. Chamberlain G, Wright K, Rot A, Ashton B, Middleton J. Murine mesenchymal stem cells exhibit a restricted repertoire of functional chemokine receptors: comparison with human. *PLoS One.* 2008;3(8):e2934.
92. Ringe J, Strassburg S, Neumann K, Endres M, Notter M, Burmester GR, Kaps C, Sittinger M. Towards in situ tissue repair: human mesenchymal stem cells express chemokine receptors CXCR1, CXCR2 and CCR2, and migrate upon stimulation with CXCL8 but not CCL2. *J Cell Biochem.* 2007;101(1):135-146.
93. Pricola KL, Kuhn NZ, Haleem-Smith H, Song Y, Tuan RS. Interleukin-6 maintains bone marrow-derived mesenchymal stem cell stemness by an ERK1/2-dependent mechanism. *J Cell Biochem.* 2009;108(3):577-588.
94. Wolfe AR, Trenton NJ, Debeb BG, Larson R, Ruffell B, Chu K, Hittelman W, Diehl M, Reuben JM, Ueno NT, Woodward WA. Mesenchymal stem cells and macrophages interact through IL-6 to promote inflammatory breast cancer in pre-clinical models. *Oncotarget.* 2016;7(50):82482-82492.
95. Zhang T, Tseng C, Zhang Y, Sirin O, Corn PG, Li-Ning-Tapia EM, Troncoso P, Davis J, Pettaway C, Ward J, Frazier ML, Logothetis C, Kolonin MG. CXCL1 mediates obesity-associated adipose stromal cell trafficking and function in the tumour microenvironment. *Nat Commun.* 2016;7:11674.
96. Sherman SE, Kuljanin M, Cooper TT, Putman DM, Lajoie GA, Hess DA. High Aldehyde Dehydrogenase Activity Identifies a Subset of Human Mesenchymal Stromal Cells with Vascular Regenerative Potential. *Stem Cells.* 2017;35(6):1542-1553.
97. Bendall SC, Hughes C, Stewart MH, Doble B, Bhatia M, Lajoie GA. Prevention of amino acid conversion in SILAC experiments with embryonic stem cells. *Mol Cell Proteomics.* 2008;7(9):1587-1597.

98. Kuljanin M, Dieters-Castator DZ, Hess DA, Postovit LM, Lajoie GA. Comparison of sample preparation techniques for large-scale proteomics. *Proteomics.* 2017;17(1-2).
99. Wessel D, Flugge UI. A method for the quantitative recovery of protein in dilute solution in the presence of detergents and lipids. *Anal Biochem.* 1984;138(1):141-143.
100. Kulak NA, Pichler G, Paron I, Nagaraj N, Mann M. Minimal, encapsulated proteomic-sample processing applied to copy-number estimation in eukaryotic cells. *Nat Methods.* 2014;11(3):319-324.
101. Cox J, Mann M. MaxQuant enables high peptide identification rates, individualized p.p.b.-range mass accuracies and proteome-wide protein quantification. *Nat Biotechnol.* 2008;26(12):1367-1372.
102. Guo F, Carter DE, Leask A. Mechanical tension increases CCN2/CTGF expression and proliferation in gingival fibroblasts via a TGFbeta-dependent mechanism. *PLoS One.* 2011;6(5):e19756.
103. Kuk H, Hutchenreuther J, Murphy-Marshman H, Carter D, Leask A. 5Z-7-Oxozeanol Inhibits the Effects of TGFbeta1 on Human Gingival Fibroblasts. *PLoS One.* 2015;10(4):e0123689.
104. Irizarry RA, Hobbs B, Collin F, Beazer-Barclay YD, Antonellis KJ, Scherf U, Speed TP. Exploration, normalization, and summaries of high density oligonucleotide array probe level data. *Biostatistics.* 2003;4(2):249-264.